Chapter 7

Condensation on External Surfaces

(This chapter was updated in 2007)

SUMMARY: The principles of film condensation on external surfaces are presented. Geometries that are addressed are: vertical plates, horizontal tubes, horizontal tube arrays, tube bundles and enhanced surfaces. The effects of vapor shear, interfacial waves, interfacial vapor shear, surface tension and non-condensable gases are addressed. The flow modes of laminar and turbulent films and intertube flow modes between tubes are discussed. Numerous methods are presented for prediction of local condensation heat transfer coefficients for plain surfaces, low finned tubes and now for an enhanced condensing tube.

7.1 Modes of Condensation

Condensation is the heat transfer process by which a saturated vapor is converted into a liquid by means of removing the latent heat of condensation. From a thermodynamic standpoint, condensation occurs when the enthalpy of the vapor is reduced to the state of saturated liquid. In practice, the process is dynamic and heat must be transferred in order to achieve condensation. Thus, condensation occurs when a vapor contacts a solid surface or a fluid interface whose temperature is below the saturation temperature of the vapor.

This chapter will deal with condensation on the ***outside of surfaces***, such as on plates, horizontal or vertical tubes and tube bundles. The following chapter provides a treatment of ***intube condensation***, in which the process takes place inside enclosed channels typically with forced flow conditions.

Four basic mechanisms of condensation are generally recognized: drop-wise, film-wise, direct contact and homogeneous. The first three are categorized as heterogeneous processes. Figure 7.1 illustrates these condensation modes. In *drop-wise condensation*, the drops of liquid form from the vapor at particular nucleation sites on a solid surface, and the drops remain separate during growth until carried away by gravity or vapor shear. In *film-wise condensation*, the drops initially formed quickly coalesce to produce a continuous film of liquid on the surface through which heat must be transferred to condense more liquid. In *direct contact condensation*, the vapor condenses directly on the (liquid) coolant surface, which is sprayed into the vapor space. In *homogeneous condensation*, the liquid phase forms directly from super-saturated vapor, away from any macroscopic surface; it is however generally assumed, in practice, that there are particles of dust or mist particles present in the vapor to serve as nucleation sites.

While drop-wise condensation is alluring because of the very high heat transfer coefficients that result, it is not considered to be suitable for deliberate employment in process equipment. Generally, special materials must be employed (of low thermal conductivity, low surface energy, low wetting or be highly polished) to attain drop-wise condensation. Hence, the process is susceptible to any fouling or oxidation of the surface that may bring the process back into the film-wise mode, with a corresponding reduction in thermal performance. Drop-wise condensation is known to occur unexpectedly in experimental test facilities since the surfaces may be new, polished and very clean, which gives much higher coefficients than for the film-wise conditions under study (some researchers hence deliberately oxidize their test surfaces to avoid the drop-wise mode). For more information on drop-wise condensation, refer for instance to Griffith (1983).

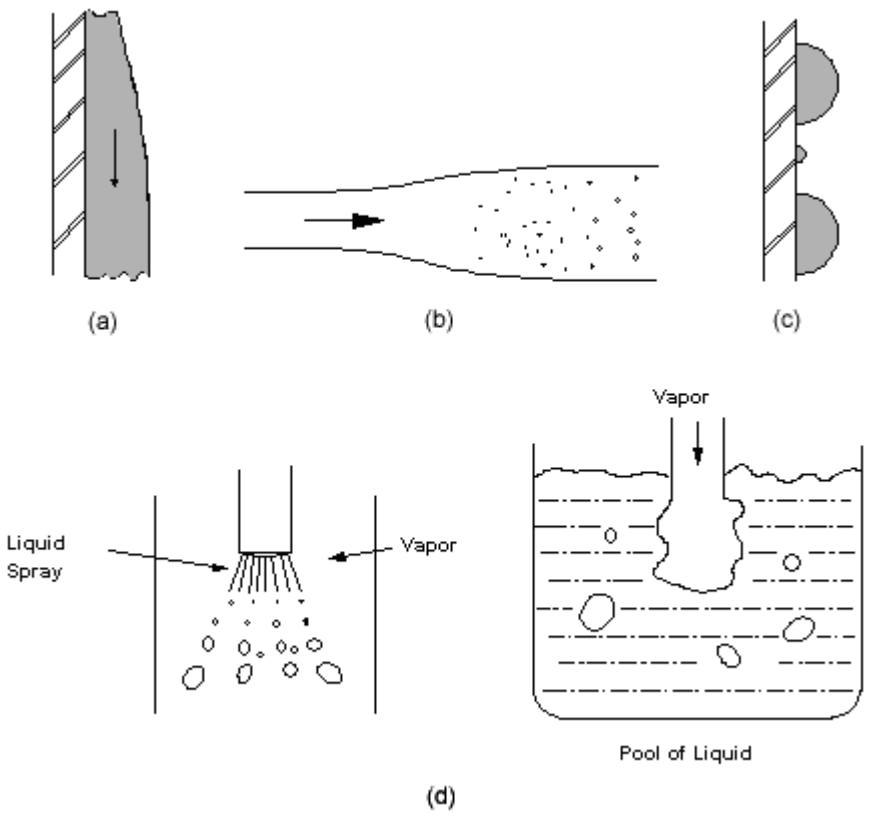

Figure 7.1. Various modes of condensation. (a) Filmwise condensation. (b) Homogenous condensation - fog formation. (c) Dropwise condensation. (d) Direct Contact Condensation

Direct contact condensation is a very efficient process, but it results in mixing the condensate with the coolant. Therefore, it is useful only in those cases where the condensate is easily separated, or where there is not desire to reuse the condensate, or where the coolant and condensate are in fact the same substance.

Condensate forming as suspended droplets or mist in a subcooled vapor is called *homogeneous* condensation, of which the most common example in nature is fog. Homogeneous condensation is primarily of concern in fog formation in equipment, i.e. to be avoided, and is not a design mode.

Film-wise condensation is the only of the above processes of particular industrial interest. Thus, all the subsequent treatment of condensation will implicitly mean film-wise condensation, in which the heat transfer surface is covered by a thin film of condensate flowing under the influence of gravity, vapor shear and/or surface tension forces. A review of recent literature is also available in Thome (1998).

7.2 Laminar Film Condensation on a Vertical Plate

7.2.1 Integral Analysis of Nusselt

Laminar film condensation of a pure single-component saturated vapor was among the first heat transfer problems to be successfully analyzed from a fundamental point of view. The definitive work is by Nusselt (1916) in two papers published two weeks apart in 1916 that has been widely described in numerous books since. The original analysis applies specifically to laminar flow of a condensing film on a vertical

surface. However, it is possible to generalize this approach to a number of other geometric cases, and for this reason it is worthwhile to examine his analysis in some detail here. The Nusselt falling film analysis closely represents experimental results on vertical plates if no ripples or non-condensable gases are present and the film flow is laminar.

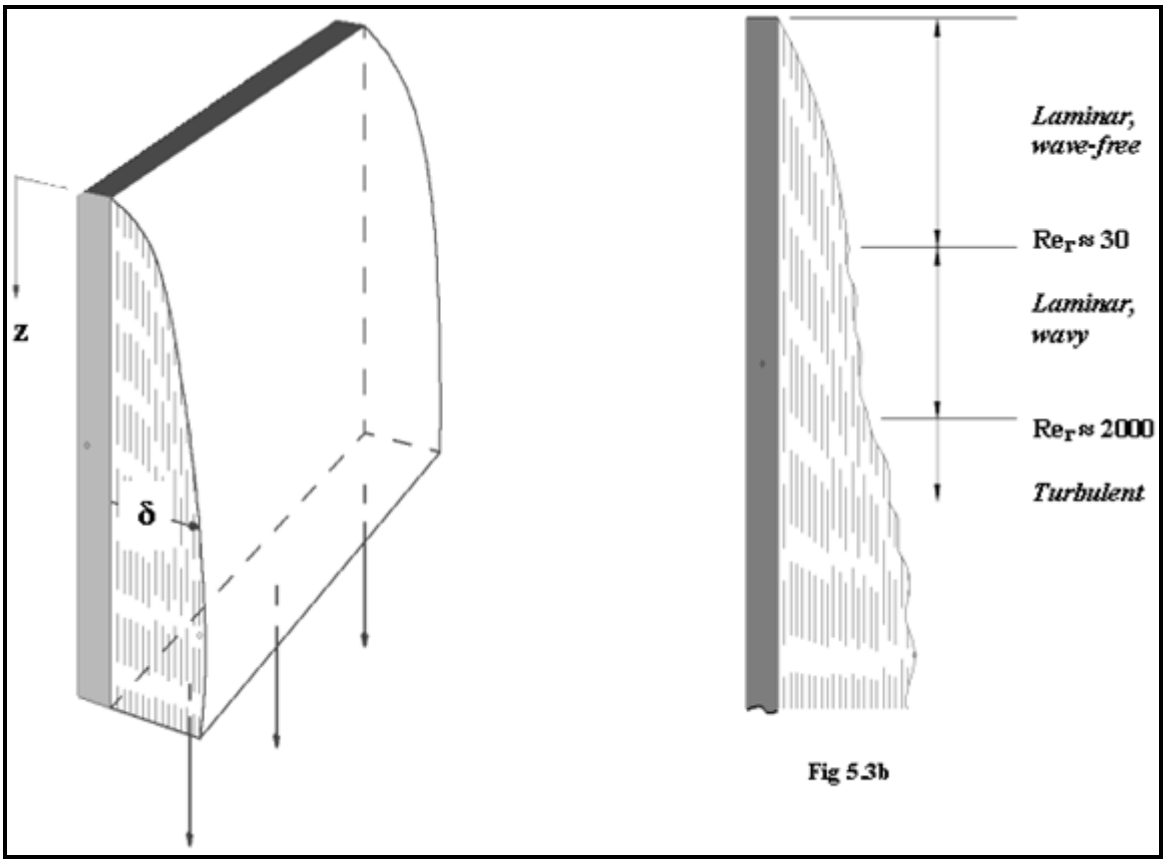

Figure 7.2. Film condensation on a vertical plate.

First of all, Figure 7.2 depicts the process of laminar film condensation on a vertical plate from a quiescent vapor. The film of condensate begins at the top and flows downward under the force of gravity, adding additional new condensate as it flows. The flow is laminar and the thermal profile in the liquid film is assumed to be fully developed from the leading edge. Thus, the temperature profile across the film is linear and heat transfer is by one-dimensional heat conduction across the film to the wall. Other assumptions in the Nusselt analysis are as follows:

- The vapor temperature is uniform and is at its saturation temperature;
- Gravity is the only external force acting on the film (momentum is neglected so there is a static force balance);
- The adjoining vapor is stagnant and does not exert drag on the film;
- Fluid properties are constant;
- The sensible cooling of the film is negligible with respect to the latent heat;
- The curvature of the interface is negligible so the saturation temperature of the interface is that of a planar interface determinable from the vapor pressure curve of the fluid.

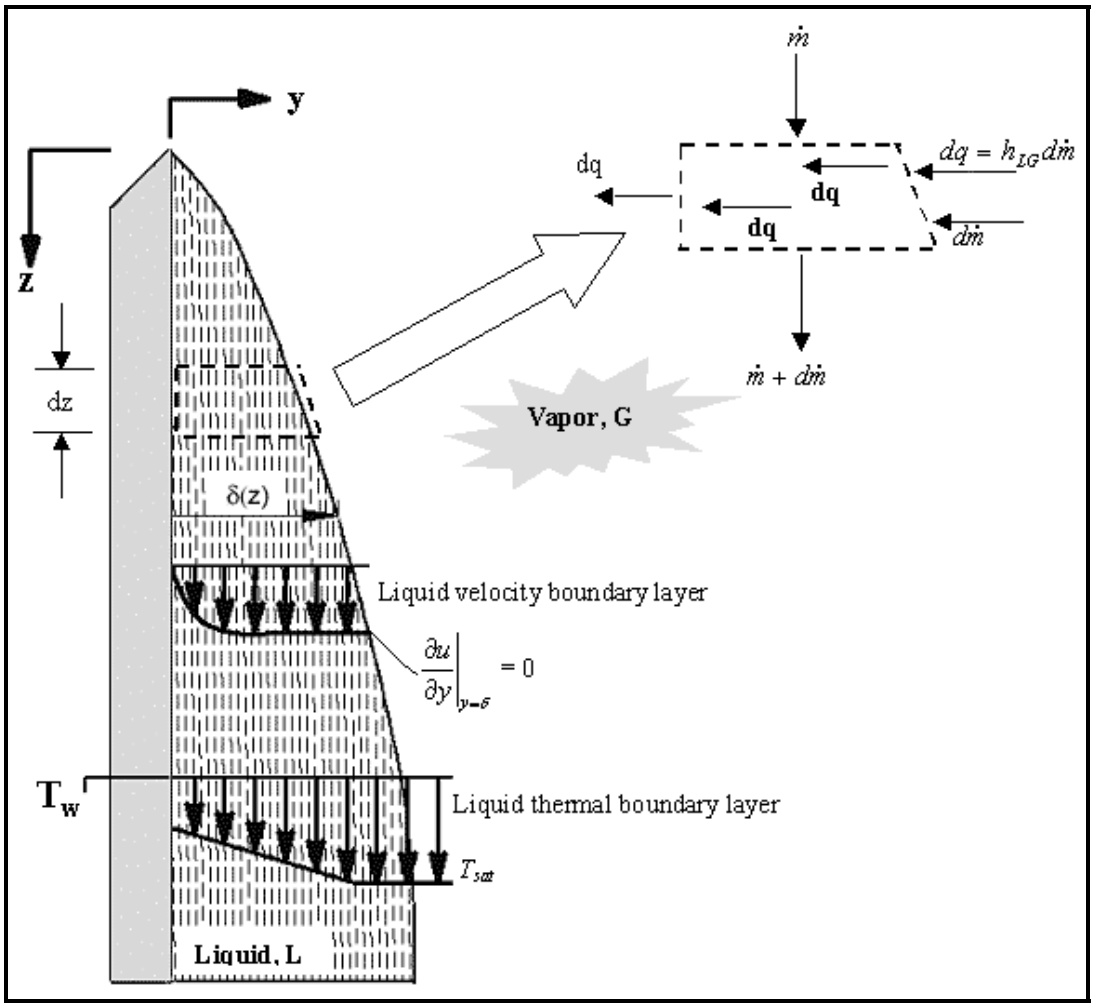

Figure 7.3. Integral representation of falling laminar film on a vertical plate.

The integral analysis of the process on a vertical plate is represented in Figure 7.3. At a distance z from the top, the thickness of the film is δ. Ignoring inertia effects, i.e. no acceleration of the flow, a force balance on the liquid element gives

$$(\delta - y)dz(\rho_L - \rho_G)g = \mu_L\left(\frac{du_y}{dy}\right)dz \qquad [7.2.1]$$

In this expression gravity acts as a body force on the element of volume (δ-y)(dz)(1) where a unit width of the plate is assumed. The viscous force is for the shear on the film at distance y from the wall over the length dz. While this expression is for a *vertical* plate, it is applicable to an *inclined* plate as long as the angle of inclination is sufficient for drainage of the condensate. For an inclined plate, the force of gravity g on the film in the above expression is replaced with g sin β, where β is the angle of the plate relative to horizontal. Now, rearranging and integrating this expression from the initial boundary condition of $u_y = 0$ at y = 0, then the velocity profile at any location y in the film is obtained to be:

$$u_y = \frac{(\rho_L - \rho_G)g}{\mu_L}\left[y\delta - \frac{y^2}{2}\right] \qquad [7.2.2]$$

Integrating this velocity profile across the film, the mass flow rate of condensate per unit width of the plate Γ is

$$\Gamma = \rho_L \int_0^{\delta} u_y dy = \frac{\rho_L(\rho_L - \rho_G)g\delta^3}{3\mu_L} \qquad [7.2.3]$$

Γ has the dimensions of kg/ms, which represents the flow rate in kg/s per unit width of the plate. Differentiating this expression with respect to δ, where $\delta = 0$ at $z = 0$, the rate of increase of the film flow rate with film thickness is

$$\frac{d\Gamma}{d\delta} = \frac{\rho_L(\rho_L - \rho_G)g\delta^2}{\mu_L} \qquad [7.2.4]$$

Taking the film surface temperature as T_{sat} and the wall temperature as T_w, the heat conducted across the liquid film element of length dz with a thermal conductivity of k_L is

$$dq = \frac{k_L}{\delta}(T_{sat} - T_w)dz \qquad [7.2.5]$$

Applying an energy balance, this rate of heat transfer by conduction is equal to the rate of latent heat removed from the vapor at the interface, which means $dq = h_{LG}\, d\Gamma$. The rate of condensation on this element ($d\Gamma$) is thus

$$d\Gamma = \frac{k_L}{\delta h_{LG}}(T_{sat} - T_w)dz \qquad [7.2.6]$$

Substituting [7.2.6] into [7.2.4], separating variables and then integrating from $\delta = 0$ at $z = 0$ gives

$$\mu_L k_L (T_{sat} - T_w)z = \rho_L(\rho_L - \rho_G)gh_{LG}\left(\frac{\delta^4}{4}\right) \qquad [7.2.7]$$

Rearranging this expression for the local film thickness, it is

$$\delta = \left[\frac{4\mu_L k_L z(T_{sat} - T_w)}{\rho_L(\rho_L - \rho_G)gh_{LG}}\right]^{1/4} \qquad [7.2.8]$$

The physical significance of the film thickness is that of the conduction length through a solid of the same thickness, seeing that is laminar film condensation the thermal resistance is only conduction from the interface to the wall. The film thickness is shown by the above expression to be directly proportional to the temperature difference (T_{sat}-T_w), such that a larger temperature difference results in a higher condensation rate.

From the thermal conductive resistance across the film, the local condensation heat transfer coefficient $\alpha_f(z)$ at any point z from the top of the plate is

$$\alpha_f(z) = \frac{k_L}{\delta} = \left[\frac{\rho_L(\rho_L - \rho_G) g h_{LG} k_L^3}{4\mu_L z(T_{sat} - T_w)} \right]^{1/4} \qquad [7.2.9]$$

Rearranging, the local Nusselt number for film condensation is obtained using z for the characteristic dimension:

$$Nu(z) = \left[\frac{\alpha_f(z)\, z}{k_L} \right] = \left[\frac{\rho_L(\rho_L - \rho_G) g h_{LG} z^3}{4\mu_L k_L (T_{sat} - T_w)} \right]^{1/4} \qquad [7.2.10]$$

Integrating [7.2.9] from z = 0 to z, the mean heat transfer coefficient for the plate up to point z is

$$\alpha_f = \frac{1}{z}\int_0^z \alpha_f(z)dz = 0.943 \left[\frac{\rho_L(\rho_L - \rho_G) g h_{LG} k_L^3}{\mu_L z(T_{sat} - T_w)} \right]^{1/4} \qquad [7.2.11]$$

Comparing the above expressions, it is seen that the mean coefficient α_f on the plate from 0 to z is 4/3 times the value of the local coefficient $\alpha_f(z)$ at z. The mean heat transfer coefficient can also be obtained from

$$\alpha_f = \frac{\Gamma(z)\, h_{LG}}{z(T_{sat} - T_w)} \qquad [7.2.12]$$

where $\Gamma(z)$ is the condensate flow rate per unit width at a distance z from the top of the plate. Combining [7.2.12] with [7.2.6] to eliminate $(T_{sat}–T_w)$, another expression for the thickness of the condensate at point z from the top is

$$\delta = \frac{k_L \Gamma(z)\, dz}{\alpha_f z d\Gamma} \qquad [7.2.13]$$

Eliminating δ by combining [7.2.13] with [7.2.3] yields the differential expression

$$\lambda_L \left[\frac{\rho_L(\rho_L - \rho_G) g}{3\mu_L} \right]^{1/3} \frac{dz}{z} = \frac{\alpha_f \Gamma^{1/3} d\Gamma}{\Gamma(z)} \qquad [7.2.14]$$

Integrating over z gives the mean heat transfer coefficient as

$$\alpha_f = 0.925 \left[\frac{\rho_L(\rho_L - \rho_G) g k_L^3}{\mu_L \Gamma(z)} \right]^{1/3} \qquad [7.2.15]$$

It is inconvenient to utilize an expression for the condensing heat transfer coefficient in terms of (T_{sat}-T_w) as in [7.2.11] since the wall temperature is unknown beforehand in heat exchanger design and results in an iterative solution procedure. For the present situation the heat transfer coefficient can also be expressed in terms of the local film Reynolds number, which at a distance z below the top of the plate is defined as

$$\mathrm{Re}_\Gamma = \frac{4\Gamma(z)}{\mu_L} \qquad [7.2.16]$$

Substituting [7.2.16] into [7.2.15] and rearranging, the mean heat transfer coefficient up to point z is

$$\frac{\alpha_f}{k_L}\left[\frac{\mu_L^2}{\rho_L(\rho_L-\rho_G)g}\right]^{1/3} = 1.47\,\mathrm{Re}_\Gamma^{-1/3} \qquad [7.2.17]$$

where the bracketed term to the left of the equal sign together with its exponent is the characteristic length. The local condensing heat transfer coefficient in terms of film Reynolds number is

$$\frac{\alpha_f(z)}{k_L}\left[\frac{\mu_L^2}{\rho_L(\rho_L-\rho_G)g}\right]^{1/3} = 1.1\,\mathrm{Re}_\Gamma^{-1/3} \qquad [7.2.18]$$

The condensing heat transfer coefficient for a laminar film is thus seen to be inversely proportional to the film Reynolds number to the 1/3 power. This can be compared, for instance, to fully developed laminar flow inside a tube in which the laminar heat transfer coefficient is independent of the Reynolds number.

Bromley (1952) extended the Nusselt theory to include subcooling of the condensate in the heat balance. Following in this line, Rohsenow (1956) showed that empirically adding a sensible heat term to the latent heat of vaporization gave reasonable results, defining an effective latent heat of evaporation as:

$$h'_{LG} = h_{LG}\left[1+0.68\left(\frac{c_{pL}\Delta T_f}{h_{LG}}\right)\right] \qquad [7.2.19]$$

where $\Delta T_f = (T_{sat}-T_w)$. The subcooling correction is typically negligible with respect to the latent heat since condensing temperature differences tend to be small.

Regarding other physical properties, Drew (1954) proposed that they be evaluated at an effective film temperature, which he gave as [T_w+ 0.25(T_{sat}-T_w)]. For small temperature differences, it is sufficiently accurate to calculate the properties at the saturation temperature. The above analysis can also be applied to the outside or inside of a vertical tube, as long as the tube diameter is much larger than δ and the effect of vapor shear remains small.

7.2.2 Boundary Layer Analysis

Sparrow and Greg (1959) applied boundary layer analysis to the problem of laminar falling film condensation. They removed the assumption of negligible momentum changes in the liquid film but, like Nusselt, they assumed that the shear exerted by the stagnant vapor on the falling film is negligible. Their solution obtains the local film heat transfer coefficient from the heat conducted from the film into the wall

$$\alpha_f(z) = \frac{q}{T_{sat} - T_w} = \frac{k_L}{T_{sat} - T_w}\left(\frac{\partial T}{\partial y}\right)_{y=0} \qquad [7.2.20]$$

by evaluating the calculated temperature profile at y=0. Their analysis gives the local Nusselt number as:

$$Nu(z) = \frac{\alpha_f(z) z}{k_L} = \left[-\theta'(0)\right] Ja_L^{1/4}\left[\frac{g\rho_L(\rho_L - \rho_G) z^3 h_{LG}}{4\mu_L k_L (T_{sat} - T_w)}\right]^{1/4} \qquad [7.2.21]$$

where the Jakob number Ja_L is defined as

$$Ja_L = \frac{c_{pL}(T_{sat} - T_w)}{h_{LG}} \qquad [7.2.22]$$

and θ′ is the first derivative of the dimensionless temperature at η = 0, defined as

$$\theta(\eta) = \frac{T_{sat} - T}{T_{sat} - T_w} \qquad [5.2.23]$$

and the dimensionless variable η is

$$\eta = c_L\, y\, z^{-1/4} \qquad [5.2.24]$$

The boundary layer solution given by [7.2.21] includes an additional term compared to the Nusselt solution given by [7.2.10], namely $[\theta'(0)\ Ja_L^{1/4}]$. For common fluids with Prandtl numbers near unity, their simulations showed that the momentum effects were negligible as assumed by Nusselt. Furthermore, the error in utilizing [7.2.11] for $Ja_L \le 0.1$ and $1 \le Pr_L \le 100$ was less than 3%. On the other hand, for fluid with very low Prandtl numbers, e.g. liquid metals, the heat transfer coefficients are predicted with the boundary layer analysis are much smaller than those given by the Nusselt solution.

7.3 Influence of Interfacial Phenomena on Laminar Film Condensation

7.3.1. Ripples and Waves

The assumption that the interface of the laminar falling film is smooth is often not true. Observations indicate that the interface becomes unstable and forms ripples or waves as shown in Figure 7.4 and Drew (1954) has pointed to them to explain the positive difference between carefully measured experimental values and those given by Nusselt theory, with up to 50% higher values in some cases. The ripples increase heat transfer by enlarging the interfacial area and by reducing the mean thickness of the film. Based on analysis of experimental observations, Brauer (1956) related the film Reynolds number Re_Γ for the onset of waves to the Archimedes number Ar_L, which is defined as

$$Ar_L = \frac{\rho_L^2 \, \sigma^{3/2}}{\mu_L^2 \, g^{1/2} (\rho_L - \rho_G)^{3/2}} \qquad [7.3.1]$$

The laminar falling film condensation heat transfer coefficient on vertical plates is enhanced when

$$Re_\Gamma > 9.3 \, Ar_L^{1/5} \qquad [7.3.2]$$

This can be used as a criterion for the onset of ripples or waves; an alternative criterion suggested elsewhere is when $Re_\Gamma > 30$. To account for the effect of waves on heat transfer, Kutateladze (1963) suggested multiplying the film Reynolds number in [7.2.18] by an empirical correction of $[0.8 \, (Re_\Gamma/4)^{0.11}]$, such that [7.2.18] becomes

$$\frac{\alpha_f(z)}{k_L}\left[\frac{\mu_L^2}{\rho_L(\rho_L - \rho_G)g}\right]^{1/3} = 0.756\,Re_\Gamma^{-0.22} \qquad [7.3.3]$$

Integrating over the film Reynolds number range from 0 to Re_Γ

$$\frac{Re_\Gamma}{\alpha_f} = \int_0^{Re_\Gamma} \frac{dRe_\Gamma}{\alpha_f(z)} \qquad [7.3.4]$$

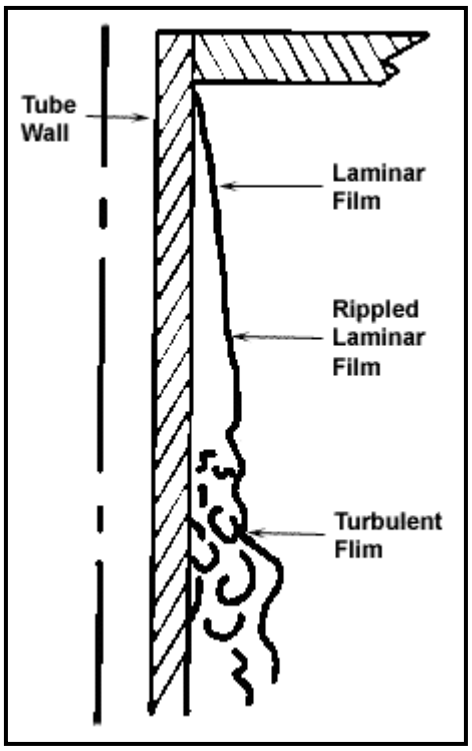

Figure 7.4. Ripples and waves on a falling film.

using expression [7.2.18] for values up to 30 and [7.3.3] for $Re_\Gamma > 30$, the resulting expression is:

$$\frac{\alpha_f}{k_L}\left[\frac{\mu_L^2}{\rho_L(\rho_L - \rho_G)g}\right]^{1/3} = \frac{Re_\Gamma}{1.08\,Re_\Gamma^{1.22} - 5.2} \qquad [7.3.5]$$

This expression is that of Butterworth (1983) and is valid up to the onset of turbulence. He noted that most experimental studies give the onset of turbulence at a film Reynolds number of about 1600. Expression [7.3.5] is solved in an iterative fashion up to the point of z in order to determine the condensate flow rate and film Reynolds number from the heat transferred.

Local expressions for the condensation heat transfer coefficient in terms of the film Reynolds number are helpful during thermal design. For example, a real plate with liquid cooling may have a non-trivial variation in $(T_{sat}-T_w)$. Similarly, a non-isothermal plate can be modeled by dividing it into successive isothermal zones, including the variation in local physical properties. Finally, calculation of the local film Reynolds number is an explicit way to determine when the laminar condensation equations are applicable or if the turbulent film flow regime has been reached.

7.3.2 Cocurrent Interfacial Vapor Shear

Interfacial shear of cocurrent vapor flow on a laminar falling film tends to thin the film and increase heat transfer. On the other hand, counter-current vapor flow would counteract the body force on the condensate and thicken the film. Nusselt analyzed condensation under the influence of cocurrent

interfacial vapor shear at high vapor velocities for a laminar liquid film and the corresponding equation to [7.2.1] for cocurrent vapor shear conditions is

$$(\delta - y)\,dz\left(\rho_L\, g \sin\beta - \left(\frac{dp}{dz}\right)\right) + \tau_i dz = \mu_L\left(\frac{du_y}{dy}\right)dz \qquad [7.3.6]$$

The inclination of the plate is included by replacing g with g sinβ where β is the inclination angle of the surface relative to horizontal. The cocurrent vapor produces an interfacial shear stress τ_i. For convenience sake, a fictitious vapor density ρ_G^* is defined:

$$\left(\frac{dp}{dz}\right) = \rho_G^*\, g \sin\beta \qquad [7.3.7]$$

If the static head of the vapor is taken as the pressure gradient, then $\rho_G^* = \rho_G$. Substituting [7.3.7] into [7.3.6] and integrating, the following relationships are obtained:

$$u_y = \frac{(\rho_L - \rho_G^*)g\sin\beta}{\mu_L}\left[y\delta - \frac{y^2}{2}\right] + \frac{\tau_i y}{\mu_L} \qquad [7.3.8]$$

$$\Gamma = \left[\frac{\rho_L(\rho_L - \rho^*{}_G)g\sin\beta\,\delta^3}{3\mu_L}\right] + \frac{\tau_i \rho_L \delta^2}{2\mu_L} \qquad [7.3.9]$$

$$\frac{d\Gamma}{d\delta} = \left[\frac{\rho_L(\rho_L - \rho_G^*)g\sin\beta\,\delta^2}{\mu_L}\right] + \frac{\tau_i \rho_L\,\delta}{\mu_L} \qquad [7.3.10]$$

Repeating the Nusselt analysis that was used to obtain [7.2.8], the corresponding expression is

$$\frac{4\mu_L\, k_L\, z(T_{sat} - T_w)}{g\sin\beta\, h'_{LG}\, \rho_L(\rho_L - \rho_G^*)} = \delta^4 + \frac{4}{3}\left[\frac{\tau_i \delta^3}{(\rho_L - \rho_G^*)g\sin\beta}\right] \qquad [7.3.11]$$

Rohsenow, Webber and Ling (1956) defined the three dimensionless variables (film thickness δ^*, distance from the leading edge z^*, and interfacial shear stress τ_i^*) to resolve this expression:

$$\delta^* = \delta\left[\frac{\rho_L(\rho_L - \rho_G^*)g\sin\beta}{\mu_L^2}\right]^{1/3} \qquad [7.3.12]$$

$$z^* = \left(\frac{4k_L\, z(T_{sat} - T_w)}{h'_{LG}\,\mu_L\,\delta}\right)\delta^* \qquad [7.3.13]$$

$$\tau_i^* = \left(\frac{\tau_i}{(\rho_L - \rho_G^*) g \sin\beta} \right) \delta^* \qquad [7.3.14]$$

and transformed [7.3.11] to

$$z^* = \delta^{*4} + \frac{4}{3} \delta^{*3} \tau_i^* \qquad [7.3.15]$$

Integrating, this gives

$$\mathrm{Nu} = \frac{\alpha_f}{k_L} \left[\frac{\mu_L^2}{\rho_L (\rho_L - \rho_G^*) g \sin\beta} \right]^{1/3} = \frac{4}{3} \frac{(\delta_z^*)^3}{z^*} + 2 \frac{\tau_i^* (\delta_z^*)^2}{z^*} \qquad [7.3.16]$$

where the corresponding film Reynolds number is

$$\frac{4\Gamma(z)}{\mu_L} = \frac{4}{3} (\delta_z^*)^3 + 2\tau_i^* (\delta_z^*)^2 \qquad [7.3.17]$$

By substituting [7.3.17] into [7.3.16], δ_z^* can be eliminated. Figure 7.5 shows this expression evaluated for cocurrent downflow by Rohsenow, Webber and Ling (1956) where the dashed lines depict the onset of turbulence in the film. As an example of the potential effect of vapor shear, at a film Reynolds number of 40 the Nusselt number is increased by about a factor of 1.5 to 6 times for the range of shear stresses simulated!

Butterworth (1981) analyzed an analogous case for the situation where the gravitational forces are negligible with respect to the interfacial shear imposed by the co-current vapor flow and laminar film flow. His dimensionless local condensation heat transfer coefficient for these conditions is:

$$\alpha_f^+(z) = 1.41 \, Re_\Gamma^{-1/2} (\tau_i^+)^{1/2} \qquad [7.3.18]$$

where the dimensionless local heat transfer coefficient is

$$\alpha_f^+(z) = \frac{\alpha_f(z)}{k_L} \left[\frac{\mu_L^2}{\rho_L (\rho_L - \rho_G) g} \right]^{1/3} \qquad [7.3.19]$$

and the dimensionless interfacial shear stress is

$$\tau_i^+ = \frac{\rho_L \tau_i}{[\rho_L (\rho_L - \rho_G) \mu_L g]^{2/3}} \qquad [7.3.20]$$

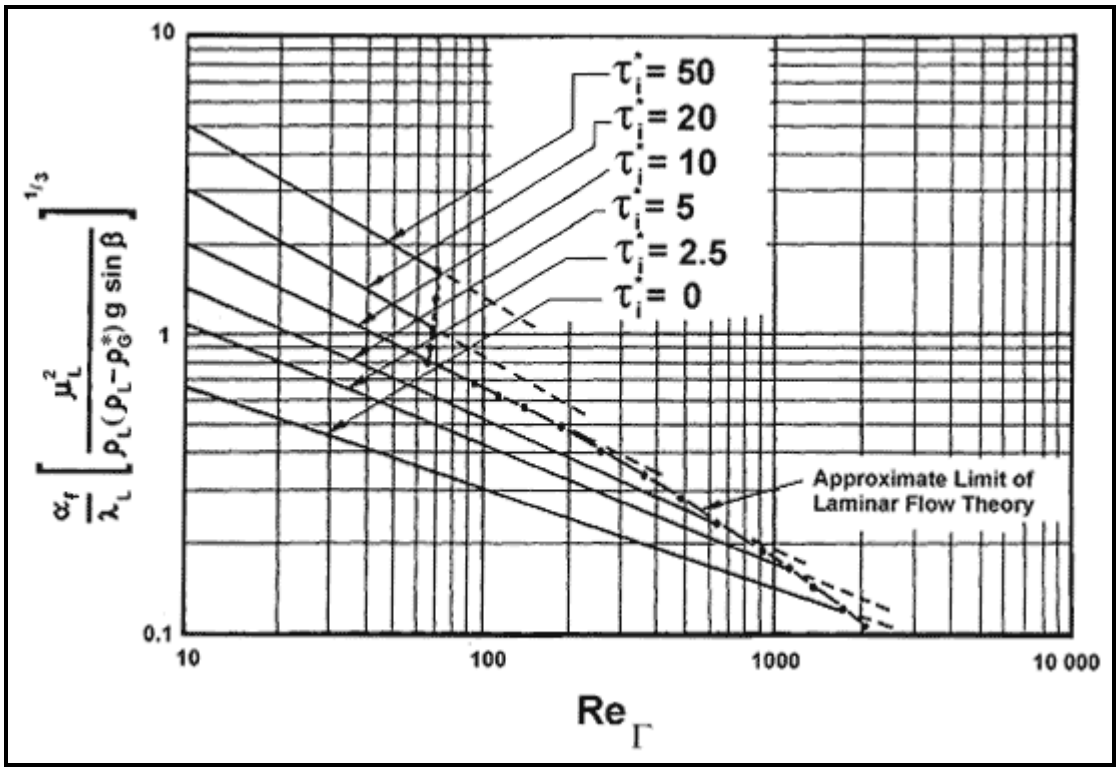

Figure 7.5. The influence of co-current vapor shear on the mean laminar falling film condensation heat transfer rate according to Rohsenow et al. (1956) [from Collier and Thome (1994)].

In his reworking of the Rohsenow, Webber and Ling (1956) analysis, low and high vapor shear effects are distinguished by use of a critical liquid film Reynolds number Re_{crit} for the onset of turbulence. An important effect of the downward interfacial shear created by the vapor is that it reduces the critical Reynolds number at which the film flow becomes turbulent. For $\tau_i^+ \le 9.04$, the critical film Reynolds number is

$$Re_{crit} = 1600 - 226\tau_i^+ + 0.667\left(\tau_i^+\right)^3 \qquad [7.3.21]$$

For $\tau_i^+ > 9.04$, Re_{crit} is a fixed value, i.e.

$$Re_{crit} = 50 \qquad [7.3.22]$$

The interfacial shear stress τ_i is

$$\tau_i = \frac{1}{2} f_i \rho_G u_{LG} \qquad [7.3.23]$$

where u_{LG} is the superficial velocity of the vapor with respect to the velocity of the film. The interfacial friction factor f_i is assumed to be that for laminar flow on a flat plate:

$$f_i = 0.664\, Re_G^{-1/2} \qquad [7.3.24]$$

where the local vapor Reynolds number is

$$Re_G = \frac{u_G z}{\nu_G} \qquad [7.3.25]$$

and z is the distance from the leading edge. Thus, depending on the local value of Re_Γ with respect to Re_{crit}, the appropriate expression is used to calculate the local heat transfer coefficient. To implement this method, [7.3.18] must be integrated from the leading edge and an energy balance performed to determine the film flow rate and hence the value of Re_Γ.

7.3.3 Combined Effects of Gravity and Interfacial Vapor Shear

When both the gravitational and interfacial vapor shear forces are significant, Butterworth (1981) recommends using a simple asymptotic expression to incorporate their respective influences:

$$\alpha = \left(\alpha_{sh}^2 + \alpha_{grav}^2\right)^{1/2} \qquad [7.3.26]$$

where α_{grav} is the heat transfer coefficient for gravity-dominated flow from one of the Nusselt expressions, such as [7.3.5], and α_{sh} is the heat transfer coefficient for shear-dominated flow, such as [7.3.16].

7.4 Turbulent Film Condensation on a Vertical Plate without Vapor Shear

The critical film Reynolds number at which a falling film becomes turbulent is still in dispute. Colburn (1934) set the transition at a film Reynolds number of 2000 when comparing his experimental data to the Nusselt theory. Applying an analogy to turbulent liquid flow in pipes, Colburn proposed the following correlation for the local condensing coefficient for turbulent film condensation on a vertical plate

$$\frac{\alpha_f(z)}{k_L}\left[\frac{\mu_L^2}{\rho_L(\rho_L-\rho_G)g}\right]^{1/3} = 0.056\,Re_\Gamma^{0.2}\,Pr_L^{1/3} \qquad [7.4.1]$$

where z is measured from the top of the isothermal plate. In applying this expression, the Nusselt expression [7.2.9] is used up to a local film Reynolds number of 2000 and then [7.4.1] is used above the value of 2000.

Labuntsov (1957) proposed a similar expression for the local condensation heat transfer coefficient when $Pr_L \le 10$:

$$\frac{\alpha_f(z)}{k_L}\left[\frac{\mu_L^2}{\rho_L(\rho_L-\rho_G)g}\right]^{1/3} = 0.023\,Re_\Gamma^{0.25}\,Pr_L^{0.5} \qquad [7.4.2]$$

There is a notable disagreement between the empirical values in these expressions.

Figure 7.6 depicts the local Nusselt number for condensation on a vertical plate without vapor shear obtained with [7.2.18], [7.3.3] and [7.4.2] for the laminar, wavy laminar and turbulent regimes, respectively. The heat transfer coefficient decreases with increasing film Reynolds number in the laminar regime but increases with increasing Reynolds number in the turbulent regime. The large jump in the heat transfer coefficient when passing from the laminar wavy regime to turbulent film flow is due to the fact that Prandtl number effects were ignored in the Nusselt laminar film theory.

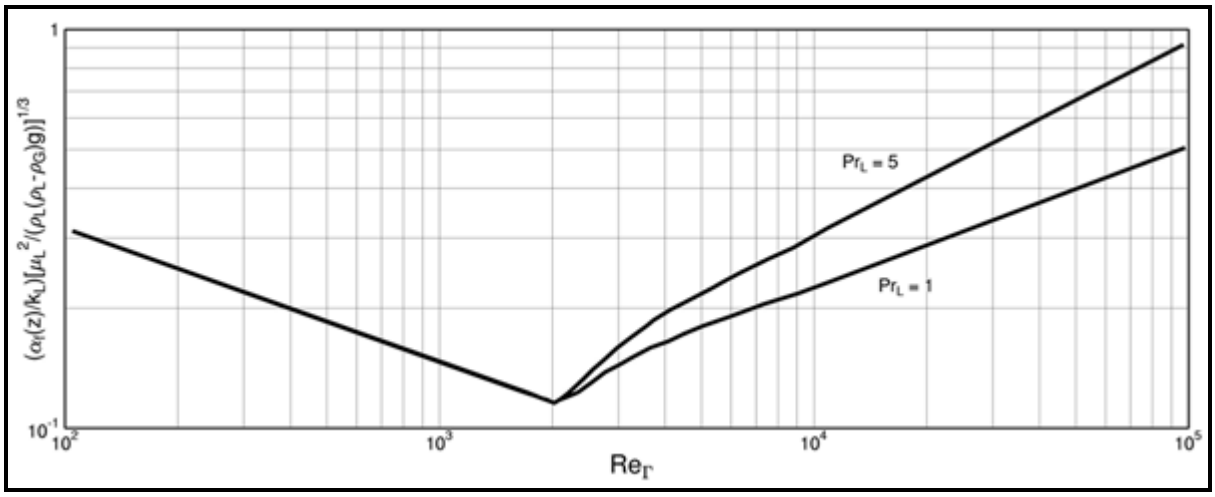

Figure 7.6. Local Nusselt numbers on a vertical plate.

Butterworth (1983) obtained the mean heat transfer coefficient over the laminar wave-free, the wavy laminar and the turbulent zones by combining [7.2.18], [7.3.3], and [7.4.2] with the help of [7.3.4]:

$$\frac{\alpha_f}{k_L}\left[\frac{\mu_L^2}{\rho_L(\rho_L-\rho_G)g}\right]^{1/3} = \frac{Re_\Gamma}{8750+58\,Pr_L^{-0.5}\left(Re_\Gamma^{0.75}-253\right)} \qquad [7.4.3]$$

This expression uses a turbulence threshold of 2000 and compares well to experimental data for condensation of steam over the range $1 < Re_\Gamma < 7200$.

The film Reynolds number threshold to turbulent film flow remains to this day in dispute. Some publications cite this occurring at a film Reynolds number as low as 1200 while others propose values of 1800 and 2000.

As an alternative to the empirical approaches above, turbulent boundary layer theory has been applied to falling film condensation by Seban (1954), Dukler (1960) and then Lee (1964) using universal velocity profiles to evaluate the eddy diffusivities in the governing boundary layer equations. A comparison of the Nusselt laminar flow theory to the Colburn, Seban and Dukler methods is depicted in Figure 7.7. Mills and Chung (1973) argued that the interface has a damping effect on large turbulent eddies in the film, such that there is a viscous sublayer at both the wall and the interface. Kutateladze (1982) arrived at the same intuitive conclusion and proposed an eddy viscosity variation that goes to zero at the wall and the interface.

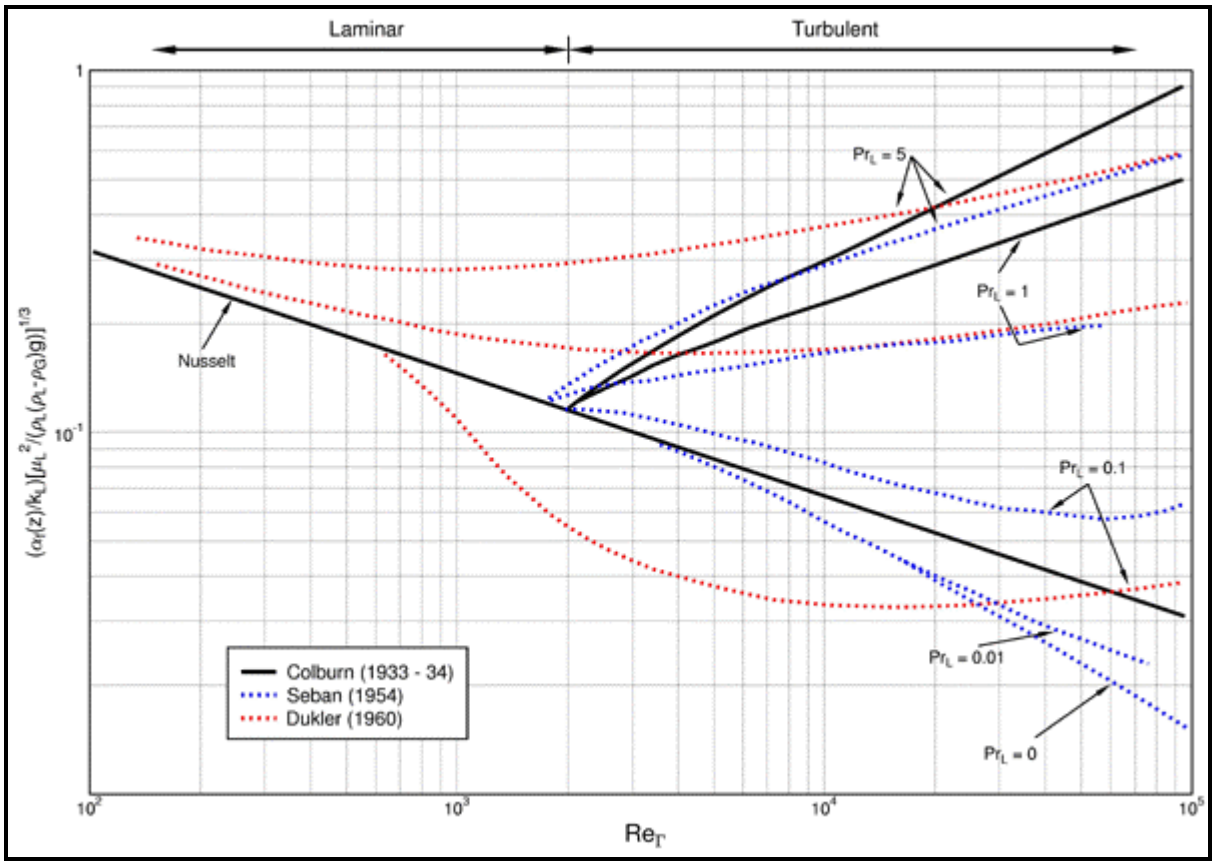

Figure 7.7. Mean Nusselt numbers predicted by various methods [from Collier and Thome (1994)].

7.5 Laminar Film Condensation on a Horizontal Tube

Applying the Nusselt integral approach to laminar film condensation on a vertical isothermal plate, the similar process on the outside of a single, horizontal isothermal tube can be analyzed. Condensation on the outside of horizontal tube bundles is often used for shell-and-tube heat exchanger applications and the first step is the analysis of a single tube. The flow is nearly always laminar on a single tube because of the short cooling length around the perimeter and is illustrated in Figure 7.8. Taking the same assumptions for the vertical isothermal plate and an integral approach for the flow, an energy balance between the one-dimensional heat conduction across the liquid film of thickness δ and the latent heat absorbed by the liquid from the condensing vapor at the interface gives

$$h_{LG}\frac{d\Gamma}{dz} = \frac{k_L\left[T_{sat}(p_G) - T_w\right]}{\delta} \qquad [7.5.1]$$

Gravitation (g sinβ) is applied around the circumference of the tube, where β is the angle around the perimeter from the top. Similar to [7.2.2] for a vertical plate, a momentum balance on this element and integration from the initial boundary condition of u = 0 at y = 0 results in the following velocity profile in the film as a function of β:

$$u_y = \frac{(\rho_L - \rho_G) g \sin\beta}{\mu_L}\left[y\delta - \frac{y^2}{2} \right] \qquad [7.5.2]$$

Integrating the velocity profile from the wall to the film interface gives the condensate mass flow rate per unit length of tube, Γ at the angle β:

$$\Gamma = \rho_L \int_0^{\delta} u_y dy = \frac{\rho_L (\rho_L - \rho_G) g \sin\beta\, \delta^3}{3\mu_L} \qquad [7.5.3]$$

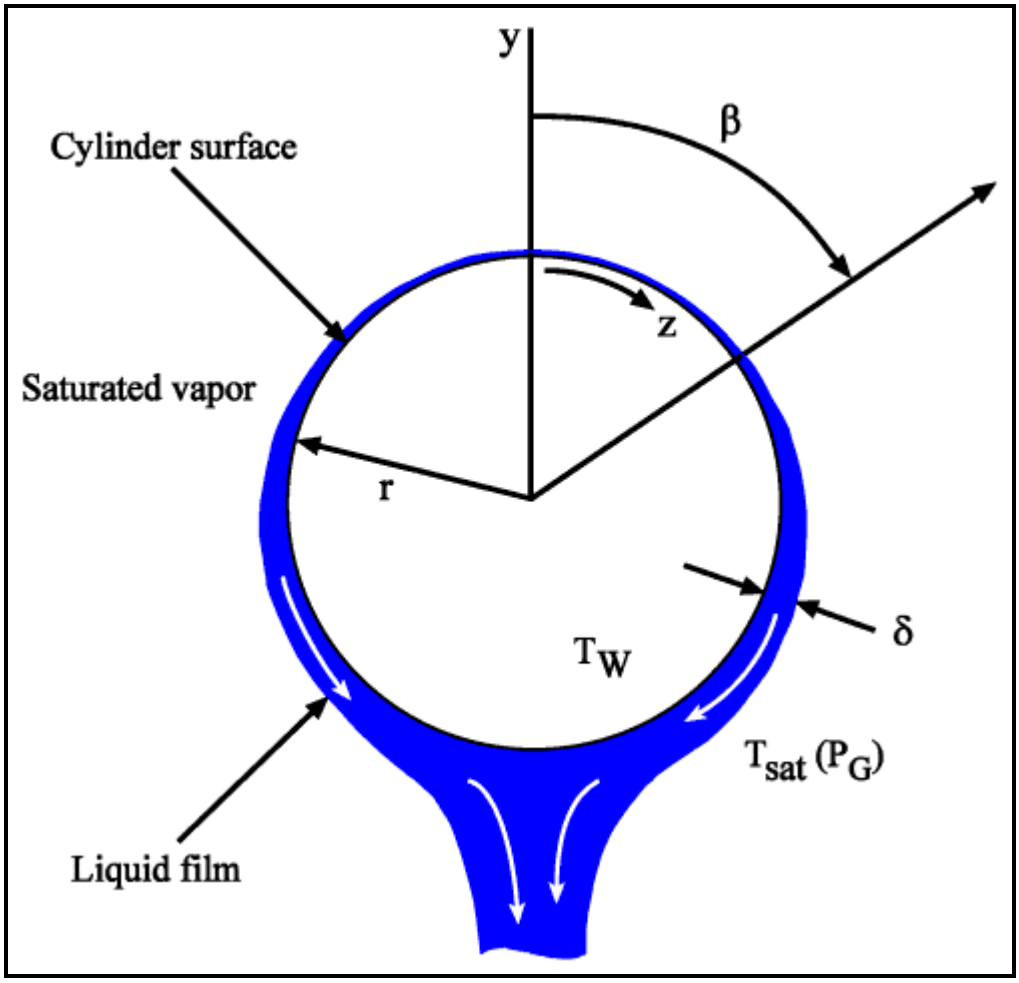

Figure 7.8. Condensation model for film condensation on a horizontal tube.

The length from to the top of the tube is z, which is related to the angle β as β = z/r, where r is the radius of the tube. Substituting into [7.5.3] and then substituting [7.5.3] into [7.5.1] yields:

$$\Gamma^{1/3} d\Gamma = \frac{r k_L (T_{sat} - T_w)}{h_{LG}}\left[\frac{(\rho_L - \rho_G) g}{3\nu_L} \right]^{1/3} \sin^{1/3}\beta \, d\beta \qquad [7.5.4]$$

Integrating from the top of the tube where $\Gamma = 0$ at $\beta = 0$ to the bottom where $\Gamma = \Gamma$ at $\beta = \pi$ gives the condensate flow rate on one side of the tube per unit axial length of tube

$$\Gamma = 1.924\left[\frac{r^3 k_L^3 (T_{sat} - T_w)^3 (\rho_L - \rho_G) g}{h_{LG}^3 \nu_L}\right]^{1/4} \qquad [7.5.5]$$

where Γ is the condensate flow rate for one side of the tube. Here, ν_L is the kinematic viscosity of the liquid. An energy balance on the circumference of the tube gives the mean heat transfer coefficient for the perimeter of the tube as

$$2h_{LG}\Gamma = 2\pi r \alpha_f (T_{sat} - T_w) \qquad [7.5.6]$$

Substituting for Γ from [7.5.5], the mean heat transfer coefficient is

$$\alpha_f = 0.728\left[\frac{\rho_L(\rho_L - \rho_G) g h'_{LG} k_L^3}{D\mu_L (T_{sat} - T_w)}\right]^{1/4} \qquad [7.5.7]$$

where D is the outside diameter of the tube. The original value of 0.725 was obtained from a numerical solution while the correct analytical value is 0.728. Heat transfer is inversely proportional to the tube diameter to the ¼ power. The mean condensate heat transfer coefficient may also be written in terms of the film Reynolds number as

$$\frac{\alpha_f}{k_L}\left[\frac{\mu_L^2}{\rho_L(\rho_L - \rho_G) g}\right]^{1/3} = 1.51 \mathrm{Re}_\Gamma^{-1/3} \qquad [7.5.8]$$

where the film Reynolds number is defined by [7.2.16]. $\Gamma(z)$ is the mass flow rate of condensate draining from the bottom of one side of the tube per unit axial length (i.e. the condensate Γ is given by [7.5.5]). This expression is valid for Re_Γ up to about 1600, which is unlikely to be exceeded on a single tube. The influence of subcooling may be incorporated by introducing [7.2.19]. The mean condensation heat transfer coefficient written in terms of the Nusselt, Rayleigh and Jakob numbers is

$$Nu_D = \frac{\alpha_f D}{k_L} = 0.728\left(\frac{Ra_L}{Ja_L}\right)^{1/4} \qquad [7.5.9]$$

The Nusselt number is written with respect to the tube diameter D. The Rayleigh number represents the ratio of the buoyancy force acting on the liquid in the film to the viscous force opposing flow while the Jakob number represents the ratio of the liquid sensible heat to the latent heat. The Jakob number Ja_L is given by [7.2.22] and the Rayleigh number Ra_L is defined as

$$Ra_L = \frac{g(\rho_L - \rho_G)\mathrm{Pr}_L D^3}{\rho_L \nu_L^2} \qquad [7.5.10]$$

The local heat transfer coefficient around the perimeter of the tube as a function of the angle β is:

$$\alpha_f(\beta) = 0.693\left[\frac{\rho_L(\rho_L-\rho_G)g\sin\beta k_L^3}{\Gamma(\beta)\mu_L}\right]^{1/3} \qquad [7.5.11]$$

Applying instead a uniform heat flux as the boundary condition around the tube rather than an isothermal temperature, Fujii, Vehara and Kurata (1972) obtained identical expressions to [7.5.7] and [7.5.8] except that the lead constants become 0.70 and 1.47, respectively. The isothermal boundary condition solution is nearly always used for thermal design.

7.6 Condensation on Horizontal Tube Bundles

In order to thermally design a shell-side condenser, the previous single tube film condensation analysis must be extended to model the process on horizontal tube bundles, which is the most widespread application of film condensation. Condensation on tube bundles raises several important considerations:

- In what manner does the condensate flow from one tube to the next?
- Is subcooling of the film important?
- Is the influence of vapor shear significant and, if so, how can this be accounted for?
- At which point does the film go through the transition from laminar to turbulent flow?

To date, these have only been partially resolved and the current knowledge will be presented below.

7.6.1 Tube Row Effect

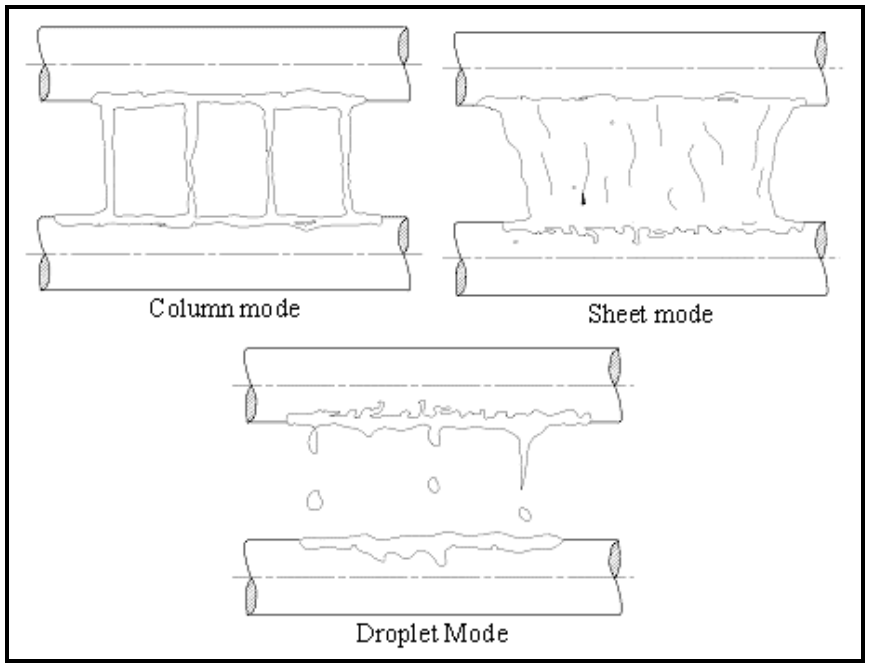

Figure 7.9. Condensation flow modes on horizontal tube arrays.

During condensation on a tube bundle, the condensate from the above tubes drains onto the tubes below, increasing the amount of condensate flowing on each tube in addition to the new condensate formed on

that particular tube. This inundation of condensate from tube row to tube row is often referred to as the tube row effect. In fact, it is more complex than just being a factor of how many tubes are located one above the other, as analyzed by Nusselt (1916) in his landmark study in which the original vertical plate Nusselt theory was presented. The tube row effect is not only dependent on how much condensate flows from tube to tube but also in what physical mode the condensate achieves this. The flow regimes formed by the condensate as it flows from one tube to that directly below it in an array of horizontal tubes are depicted schematically in Figure 7.9. The regimes encountered are described as follows for increasing film mass flow rate:

- **Droplet mode**. The liquid flows from tube to tube as individual droplets, often in rapid succession at uniform intervals along the bottom of the upper tube. The droplets range in size depending on the properties of the fluid, primarily density difference, surface tension and liquid viscosity. The droplets essentially form a jet that impinges on the lower tube. The droplets form because a continuous film on the bottom of a tube becomes unstable as a result of the Kelvin-Helmholtz instability, which causes liquid droplets to be formed at characteristic wavelengths such that droplet jets are formed at nearly equal intervals along the bottom of the tube.

- **Column mode**. At higher flow rates, the jets of droplets coalesce to form individual liquid columns that extend from the bottom of the upper tube to the top of the lower tube. The liquid columns hit the top of the lower tube as impinging jets and spread along the tube while flowing on around towards the bottom as shown in Figure 7.10 adapted from Mitrovic (1986), in which the columns are staggered from one tube row to the next. The columns may also be inline, one above the other in each successive tube row.

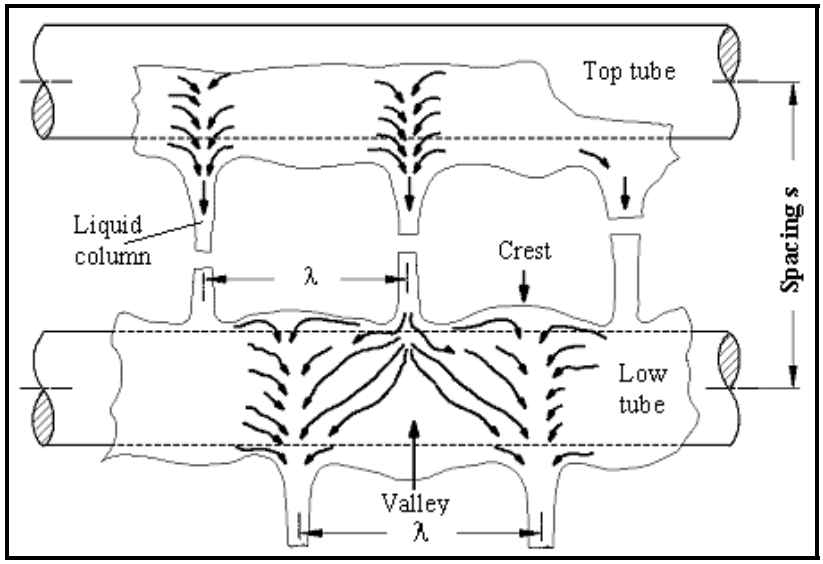

Figure 7.10. Condensate spreading over the tube for column type of condensate drainage.

- **Sheet mode**. At even higher flow rates, the columns become unstable and form short patches of liquid sheets that flow from one tube to the next. Eventually, with enough liquid, these unstable sheets join together to form more or less one continuous sheet of liquid falling from the upper tube to the lower one. This occurs only if the intertube spacing is small enough to prevent breakup of the sheet. For staggered tube arrays, if the column sheet is unstable, it may attach to the side of the next lower out-of-line tube without reaching the top of the next inline tube. Waves or ripples are typically noticeable on the flowing sheets.

- **Spray mode**. Under vapor shear conditions with its complex flow field around tubes, the above flow modes may be interrupted and the liquid carried away by the vapor. In this case, there is significant entrainment of liquid droplets into the vapor flowing between the tubes and hence a spray flow is formed. Any liquid flowing from one tube to another does so in a very chaotic manner. For staggered tube arrays, the vertical tube spacing is quite large and these liquid columns and droplet jets are easily influenced by vapor buffeting, especially where the vapor's boundary layer detaches from the sides of the tubes in vortices and in the recirculating flow regions behind the tubes. At high vapor flow rates, a large fraction of the liquid is entrainment as small liquid droplets, resulting in very thin liquid films on the tubes.

For an actual view of these intertube flow modes, which may be thought of as shell-side falling film two-phase flow regimes, Figure 7.11 depicts the three modes (droplet, column and sheet) and their two transitions. The images were taken with a high-speed digital video camera. The columns in this case are inline but staggered columns also occur as mentioned above.

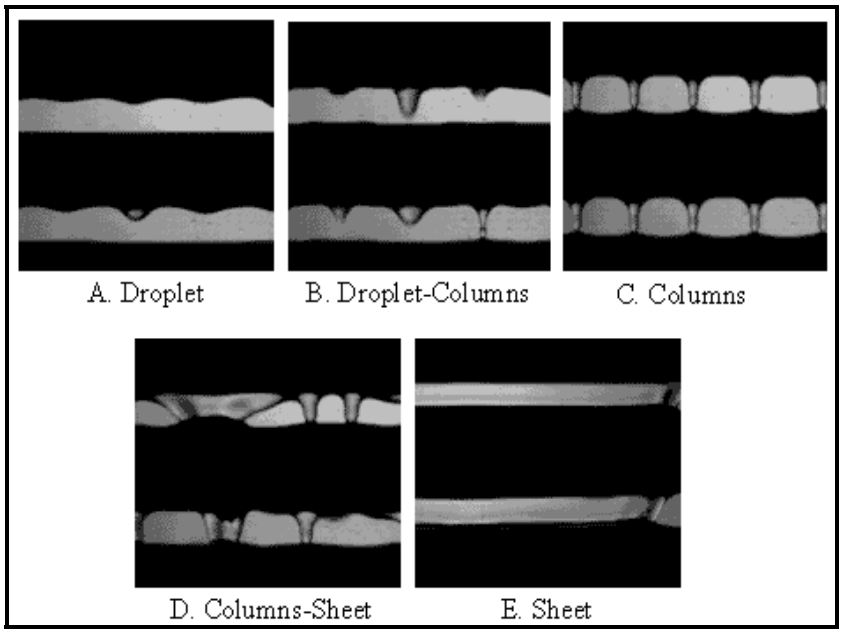

Figure 7.11. Video images of three flow modes and their transitions [images courtesy of Laboratory of Heat and Mass Transfer, Swiss Federal Institute of Technology Lausanne].

The Nusselt equation for a single tube may be extended to a vertical array of horizontal tubes, i.e. horizontal tubes situated one above the other, assuming that the sheet mode exits in between all the tubes. Essentially, this is equivalent to assuming that there is an embossed vertical plate of half-tubes with no gap between the tubes with the condensate flowing from one to another. Starting with [7.5.8], the analysis is applied to each individual tube utilizing the summation of the condensate flowing from the above tubes onto the top of the Nth tube, counting the tubes from the top row towards the bottom. Applying an energy balance to the entire surface area of the array of tubes yields

$$2\pi rN\alpha\left(T_{sat} - T_w\right) = 2h_{LG}\left[\Gamma_{bottom}(N)\right] \qquad [7.6.1]$$

where α is the mean condensation heat transfer coefficient for all the tubes, N is the number of tubes in the vertical array, h_{LG} is the latent heat and $\Gamma_{bottom}(N)$ is the total flow rate of condensate off the bottom tube from one side per unit length of tube. The mean condensation heat transfer coefficient for N tubes of diameter D is

$$\frac{\alpha(ND)}{k_L} = 0.728\left[\frac{g(\rho_L - \rho_G)(ND)^3 h_{LG}}{k_L \nu_L (T_{sat} - T_w)}\right]^{1/4} \qquad [7.6.2]$$

The mean heat transfer coefficient in terms of the film Reynolds number for the condensate leaving the bottom of the Nth tube is

$$\frac{\alpha}{k_L}\left[\frac{\mu_L^2}{\rho_L(\rho_L - \rho_G)g}\right]^{1/3} = 1.92\left(\frac{4\Gamma(N)}{\mu_L}\right)^{-1/3} \qquad [7.6.3]$$

where the flow rate of condensate draining from one side of the Nth tube is

$$\Gamma(N) = \frac{N\pi D\alpha(T_{sat} - T_w)}{h_{LG}} \qquad [7.6.4]$$

The mean condensation heat transfer coefficient α, for an entire array of tubes is:

$$\frac{\alpha}{\alpha(N=1)} = N^{-1/4} \qquad [7.6.5]$$

where $\alpha(N=1)$ is the heat transfer coefficient for the top tube row, i.e. the original Nusselt equation for a single tube given by [7.5.7] and [7.5.8]. This method is applicable if the film flow remains *laminar* all the way to the bottom of the Nth row. The heat transfer coefficient on the Nth tube row in the bundle $\alpha(N)$ is

$$\frac{\alpha(N)}{\alpha(N=1)} = N^{3/4} - (N-1)^{3/4} \qquad [7.6.6]$$

Kern (1958) concluded from his practice experience in designing condensers that the above tube row expression was too conservative and that this resulted in condensers that were consistently over-surfaced. To improve his thermal designs, he replaced the exponent of (-1/4) in expression [7.6.5] with a value of (-1/6) so that corresponding equations become

$$\frac{\alpha}{\alpha(N=1)} = N^{-1/6} \qquad [7.6.7]$$

$$\frac{\alpha(N)}{\alpha(N=1)} = N^{5/6} - (N-1)^{5/6} \qquad [7.6.8]$$

These equations are presently widely used in the thermal design of condensers. Figure 7.12 presents a comparison of experimental data from different sources compiled by Marto (1986) with respect to the

Nusselt and Kern tube row methods. The wide bandwidth of the data compared to the two curves may be some vapor shear effects in the data but is more likely the influence of intertube flow mode types encountered during the experiments, i.e. the modes described above. Experiments have shown that most data are equal to, or higher than, those given by Nusselt's sheet flow analysis. The discrepancy arises because the type of flow has an effect on the analysis. For example, if the flow mode is column-wise, then a portion of the lower tubes will perform without condensate inundation, while the rest of the tube surface will suffer more inundation than in the sheet mode. Hence, the performance will change accordingly. Overall, the column mode is thought to have a positive influence on heat transfer. Therefore, the Nusselt's sheet mode solution is the lower limiting case for the tube row effect. Heat transfer in the other two modes (column and droplet) is expected to be higher.

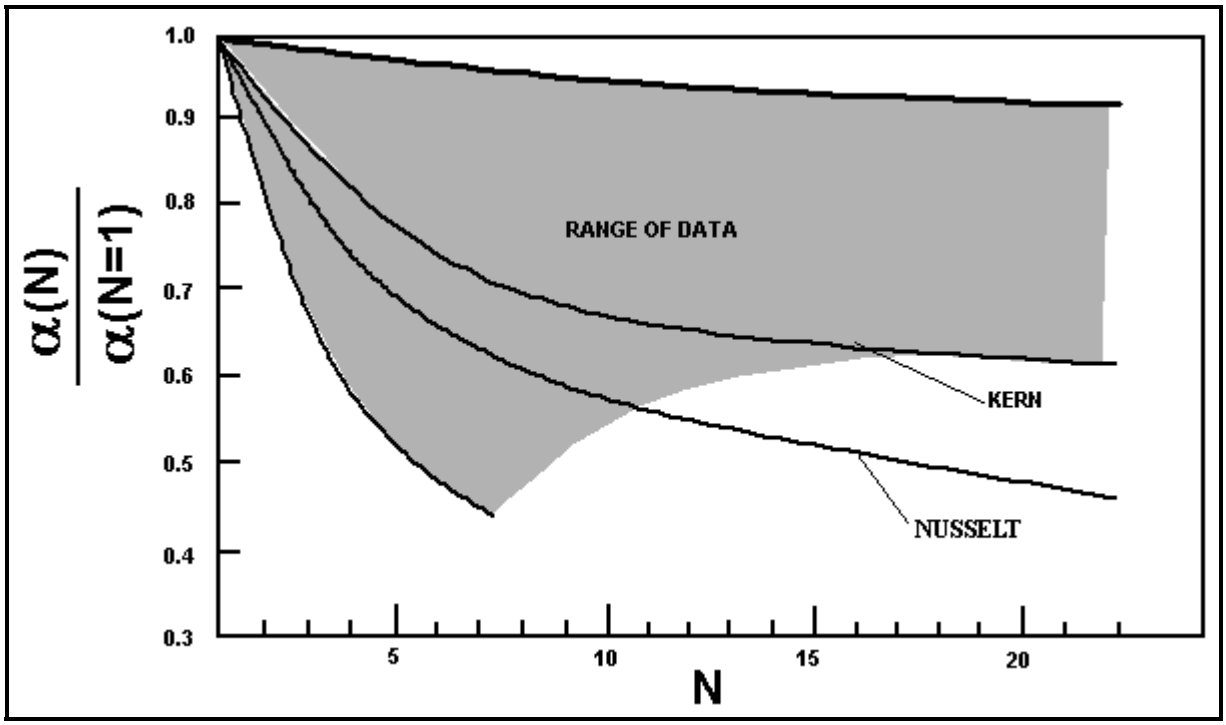

Figure 7.12. Competing tube row methods for condensation on a vertical array of tubes compared to experimental results from Marto (1986).

It is important to understand that these tube row expressions are applied in practice by counting the number of vertical inline tube rows. Hence for an inline or square tube layout, each tube row from the top to the bottom of the bundle is counted in applying these equations. Instead, for staggered tube layouts the condensate is normally assumed to flow to the next inline tube row since it cannot flow onto the top of the out-of-line tube in the next lower row. Thus, the total number of tube rows to use is one-half the actual number, which naturally means that staggered layouts are more advantageous for heat transfer. Since some condensate in a staggered bundle ends up on the sides of the next out-of-line tubes, this assumption is a little optimistic as shown in Figure 7.13 adapted from Marto (1986). Hence, the total number of vertical tube rows in a staggered tube bundle are somewhere between the number of inline rows and the total number of staggered rows, and an average of these two values may be used as a reasonable approximation.

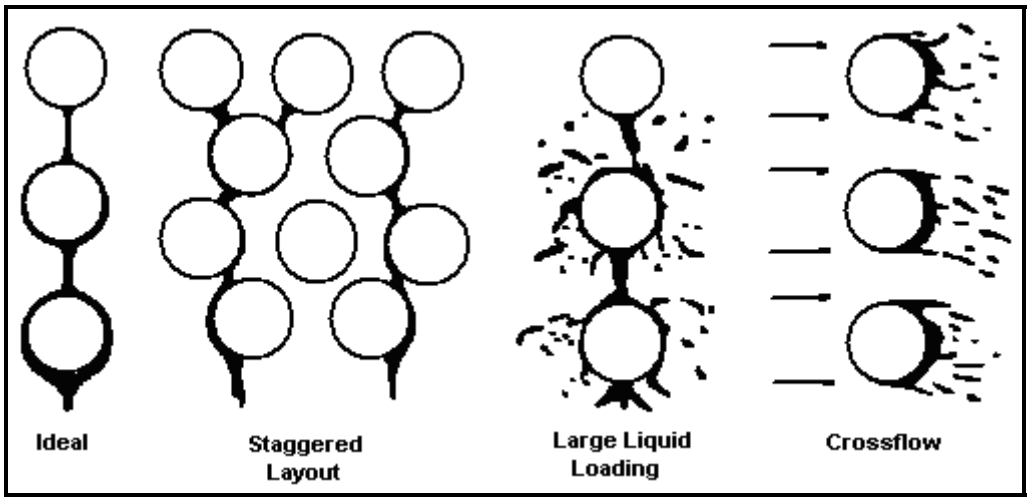

Figure 7.13. Illustration of realistic flow of liquid on tube bundle.

7.6.2 Falling Film Flow Regime Transitions on Tube Arrays

At this date, no generalized falling film mode transition map is apparently available for condensation conditions. Honda, Nozo and Takeda (1987) notably, however, has proposed several transition expressions for several refrigerants condensing on low finned tubes. This process is very similar to that of an adiabatic film of liquid falling on a tube array, which has been studied by Hu and Jacobi (1996a) for a variety of fluids, tube diameters, tube pitches and flow rates and with/without cocurrent gas flow and by Mitrovic (1986) as a function of tube spacing, all for plain tubes. More recently by Roques, Dupont and Thome (2002) and Roques and Thome (2001, 2002) have run tests with water, glycol and one water-glycol mixture for one plain tube, then 19 fpi, 26 fpi and 40 fpi low fin tubes, and finally two enhanced tubes (Turbo-Bii and Thermoexcel-E). The 26 fpi tube studied was a Wolverine Turbo-Chil tube.

Hu and Jacobi (1996a) proposed flow mode transition equations with Re_Γ versus Ga_L (film Reynolds number vs. the Galileo number) for the following principal flow modes: sheet flow, column flow and droplet flow. The mixed mode transition zones of column-sheet and droplet-column were also considered as regimes, bringing the total to five. Hence, they presented four flow transition expressions (valid for passing through the transitions in either direction and hence the symbol ⇔):

Droplet⇔Droplet-Column:

$$Re_\Gamma = 0.148\, Ga_L^{0.302} \qquad [7.6.9]$$

Droplet-Column⇔Column:

$$Re_\Gamma = 0.192\, Ga_L^{0.301} \qquad [7.6.10]$$

Column⇔Column-Sheet:

$$Re_\Gamma = 2.828\, Ga_L^{0.233} \qquad [7.6.11]$$

Column-Sheet⇔Sheet:

$$Re_{\Gamma} = 2.896\, Ga_L^{0.236} \qquad [7.6.12]$$

The film Reynolds number Re_Γ in their original publication was for flow down *one side* of the tube; hence, the above expressions are evaluated using the film Reynolds number definition given by [7.2.16] with flow down *one side* of the tube to conform to the situation here. The Galileo number Ga_L is defined as

$$Ga_L = \frac{\rho_L \sigma^3}{\mu_L^4 g} \qquad [7.6.13]$$

Figure 7.14 depicts these expressions as a flow transition map, applicable only to plain tubes and air velocities less than 15 m/s.

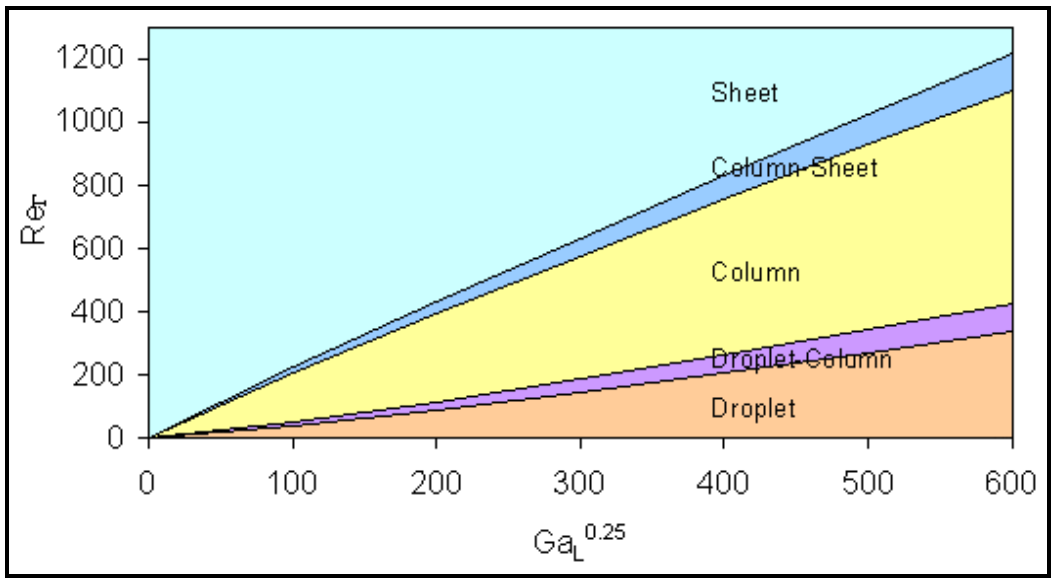

Figure 7.14. Flow mode map for falling film flow on a vertical array of horizontal tubes.

Honda, Nuzo and Takeda (1987) have looked at some of the transitions in flow modes on a low finned tube for one refrigerant. More recently, Roques, Dupont and Thome (2002) and Roques and Thome (2001) have reported transition curves similar to those above for plain tubes, low finned tubes (19, 26 and 40 fpi tubes), Thermoexcel-C and Turbo-Bii tubes. They observed that the low finned tubes and the enhanced condensing Thermoexcel-C tube had some significantly different transition thresholds, primarily enlarging the range of conditions at which the column mode exists, which is positive from a heat transfer perspective. These types of studies will eventually lead to condensation design methods in which the tube row effect includes the flow mode effect.

7.6.3 Vapor Shear Effects on Tube Bundles

Vapor shear manifests its influence on the condensation process in tube bundles primarily in three ways. First of all, it has an effect of the film flow, tending to increase heat transfer by thinning the film, similar to its effect on vertical plates described earlier. Secondly, the interfacial shear may remove the film from the tube wall, similar to the transition from annular flow to mist flow inside a tube at high vapor core velocities. Thirdly, the vapor shear modifies the intertube flow modes. For instance, the sheet mode is not stable in presence of high velocity vapor and will be broken up into droplets, creating a mist flow. In a

condenser, high vapor velocities may exist near the inlet. Deeper into the bundle, however, the vapor velocity decreases rapidly as the vapor condenses.

McNaught (1982) has estimated the shear-controlled heat transfer coefficient α_{sh} for the situation where the vapor shear force is dominant and the gravity force on the film is negligible as

$$\alpha_{sh} = 1.26(1/X_{tt})^{0.78}\alpha_L \qquad [7.6.14]$$

In this expression the liquid film heat transfer coefficient α_L is determined assuming that the liquid phase occupies the entire flow channel, i.e. the liquid fraction of the total flow at the minimum cross-sectional area of the bundle, and flows as a turbulent liquid across the bundle. The value of α_L can be determined from correlations for crossflow heat transfer over tube bundles found in textbooks. The Martinelli parameter X_{tt} he used is

$$X_{tt} = \left(\frac{1-x}{x}\right)^{0.9}\left(\frac{\rho_G}{\rho_L}\right)^{0.5}\left(\frac{\mu_L}{\mu_G}\right)^{0.1} \qquad [7.6.15]$$

where x is the vapor quality. To find the combined effect of gravity controlled condensation and vapor-shear controlled condensation, the gravity-controlled heat transfer coefficient α_{grav} is calculated with the Nusselt single tube expression [7.5.7] together with the inundation tube row effect. For staggered and inline layouts, he proposed the following expression

$$\alpha_{grav} = \alpha(N=1)\left[\frac{\Gamma(N-1)+\Gamma_N}{\Gamma_N}\right]^{-\gamma} \qquad [7.6.16]$$

where Γ(N-1) is the total condensate flow rate from one side of the above tubes onto the Nth tube and Γ_N is the condensation rate on one side of the Nth tube itself, whose values may be obtained with [7.6.4]. The heat transfer coefficient for the top tube row is α(N=1). The empirical exponent γ is 0.13 for triangular tube layouts and 0.22 for square tube layouts, respecting the larger tube row effect anticipated for the inline tube rows in the square layout, based on a relatively small database. Asymptotic approaches are often used for modeling the combined effects of two different mechanisms on heat transfer on heat transfer and in this case McNaught uses the expression

$$\alpha = \left(\alpha_{sh}^2 + \alpha_{grav}^2\right)^{1/2} \qquad [7.6.17]$$

where the above two expressions are used to determine the vapor-shear controlled and the gravity-controlled coefficients.

A more detailed method has been proposed by Honda et al. (1989) for condensation on inline and staggered tube bundles of plain tubes using an asymptotic model to the 4th power. Refer to that paper, or a summary of it in Collier and Thome (1994), for more information on that method.

7.6.4 Onset of Turbulence and Turbulent Film Heat Transfer

Turbulent flow of the condensate film may be reached in a condenser, which significantly increases heat transfer. Comparatively little has been published on turbulent film condensation on tube bundles

compared to the information available for laminar films. Butterworth (1983) recommends adapting the Labuntsov expression [7.4.2] for turbulent film condensation on a vertical plate to horizontal tubes for predicting local turbulent film condensation on the Nth tube row in horizontal tube bundles:

$$\frac{\alpha(N)}{k_L}\left[\frac{\mu_L^2}{\rho_L(\rho_L-\rho_G)g}\right]^{1/3} = 0.023\left(\mathrm{Re}_\Gamma/2\right)^{0.25}\,\mathrm{Pr}_L^{0.5} \qquad [7.6.18]$$

The film Reynolds number is obtained using [7.2.16] with the condensate flow rate on one side of the Nth tube in order to conform to the same definition used for turbulent condensation on a vertical plate. The transition film Reynolds number for the tube bundle is adapted from a vertical plate turbulent transition criterion of 1600 (but also values of 1200, 1800 and 2000 have been proposed) for a film on a plate to one side of a tube. Thus, the film will become turbulent on the tube bundle at Re_Γ equal to 1600 and thus for values larger than 1600 the above expression should be used.

Similar to the above theory for vertical plates covering laminar and turbulent condensation all in one integrated expression, Honda et al. (1989) achieved the same objective for arrays of horizontal tubes but by a different approach…they assumed an asymptotic model to cover the combined regime effects. For predicting their data for condensation of R-113 (without vapor shear) on a vertical column of inline horizontal tubes, their 4th order asymptotic expression for the condensation heat transfer coefficient on the Nth tube from the top row is:

$$\frac{\alpha(N)}{k_L}\left[\frac{\mu_L^2}{\rho_L(\rho_L-\rho_G)g}\right]^{1/3} = \left[\left(1.2\,\mathrm{Re}_\Gamma^{-0.3}\right)^4 + \left(0.072\,\mathrm{Re}_\Gamma^{0.2}\right)^4\right]^{1/4} \qquad [7.6.19]$$

The Reynolds number is defined as above using [7.2.16] for the local condensate flow rate on one side of the tube row. The first term on the right side of the equation is the Nusselt solution for a horizontal tube including the enhancement factor for the surface waves from Kutateladze and Gogonin (1979). The second term on the right is a correlation for turbulent condensation, similar to the expression of Colburn (1934). However, the experimental data of Honda et al. (1989) did not cover the turbulent flow regime so they used the R-12 and R-21 data of Kutateladze and Gogonin (1979) to develop that expression, which does not however explicitly include the effect of the liquid Prandtl number.

Gstöhl and Thome (2006b) have modified the Honda expression slightly to better fit their plain tube R-134a data and to explicitly include the liquid Prandtl number effect, arriving at the following expression:

$$\frac{\alpha(N)}{k_L}\left[\frac{\mu_L^2}{\rho_L(\rho_L-\rho_G)g}\right]^{1/3} = \left[\left(1.2\,\mathrm{Re}_\Gamma^{-0.3}\right)^4 + \left(0.04\,\mathrm{Re}_\Gamma^{0.2}\,\mathrm{Pr}_L^{1/3}\right)^4\right]^{1/4} \qquad [7.6.20]$$

This modified-Honda expression captured their R-134a data very well, predicting 80% of the data to within ±10%, as long as all the condensate remained on the tube row and was not slung off, giving a minimum in the heat transfer coefficient at about a Reynolds number of 300, as opposed to a much larger transition value for a vertical plate reported earlier. Interestingly, on the lower tubes of their 10 row array run with and without liquid overfeed, Gstöhl and Thome (2006b) observed that a significant amount of condensate was slung off the array by the oscillations of the falling film as it flowed from tube row to tube row. For these conditions, they found experimentally that the heat transfer coefficient was almost constant for Reynolds numbers above 300, which suggests that this liquid slinging process must be accounted for in modeling the process. According to them, the onset of slinging begins when the

maximum deflection angle of the condensate from tube to tube is larger than that of the arc subtended by the next lower tube, such that some of the oscillating condensate misses the lower tube and only a portion of the condensate is deposited on the lower tube. This effect reduces the amount of condensate flowing from tube to tube. Since they measured heat transfer coefficients that rose only slightly with increasing Reynolds numbers above 300, this insinuates that the amount of condensate slung off a tube row is about equal to the new condensate formed on it. The maximum angle of deflection θdef for a plain tube row was found empirically to be given in terms of the Reynolds number as follows:

$$\theta_{def} = 0.048\,\mathrm{Re}_{\Gamma} \qquad [7.6.21]$$

The critical angle θcrit is given by the geometry of the tube row, where S is the vertical tube pitch from tube center to tube center, to be

$$\theta_{crit} = \arcsin\left(\frac{D/2}{S-(D/2)}\right) \qquad [7.6.22]$$

In this case, the hypotenuse of the right triangle is S – D/2 (from the bottom point of the upper tube to the center of the lower tube), D/2 is the radius of the tube and θcrit is the angle of the tangent line from the bottom of the upper tube that touches the side of the lower tube. Liquid is slung off the tube array when the film Reynolds number is large enough so that θdef > θcrit. Gstöhl and Thome (2006b) also proposed a prediction method for condensation accounting for the influences of the slinging effect and the tube pitch for laminar film condensation, but it is based so far on results for only one fluid (R-134a) and one tube diameter (18.91 mm). It is planned to extend this method to include turbulent films and neighboring tube row effects in the near future while also enlarging the database to additional fluids.

7.7 Condensation on Low Finned Tubes and Tube Bundles

Integral low finned tubes have been utilized for enhancing condensation for more than half a century. The geometry of a low finned tube is illustrated in Figure 7.15 and a photograph is shown in Figure 7.16. These tubes have their fins formed by typically three sets of rings of increasing diameter that are forced into the tube wall as the tube is pulled through the ring assemblies. The fins form in the spaces between the rings and hence the term “integral”. The low finned tubes used for condensation typically have a fin tip diameter nearly identical to the diameter of plain ends of the tube such that they are easily inserted through tube sheets into tube bundles. The fins are helical around the tube with a small axial pitch. For condensation, the optimum fin density depends on the particular fluid, primarily the surface tension, and varies from 19 fins/in. (19 fpi or 748 fins/m) up to 42 fpi (1653 fins/m). Fin heights depend on the fin density and the particular tube metal, ranging from about 0.66 to 1.50 mm (0.026 to 0.059 in.). The most typical fin thickness is 0.305 mm (0.012 in.).

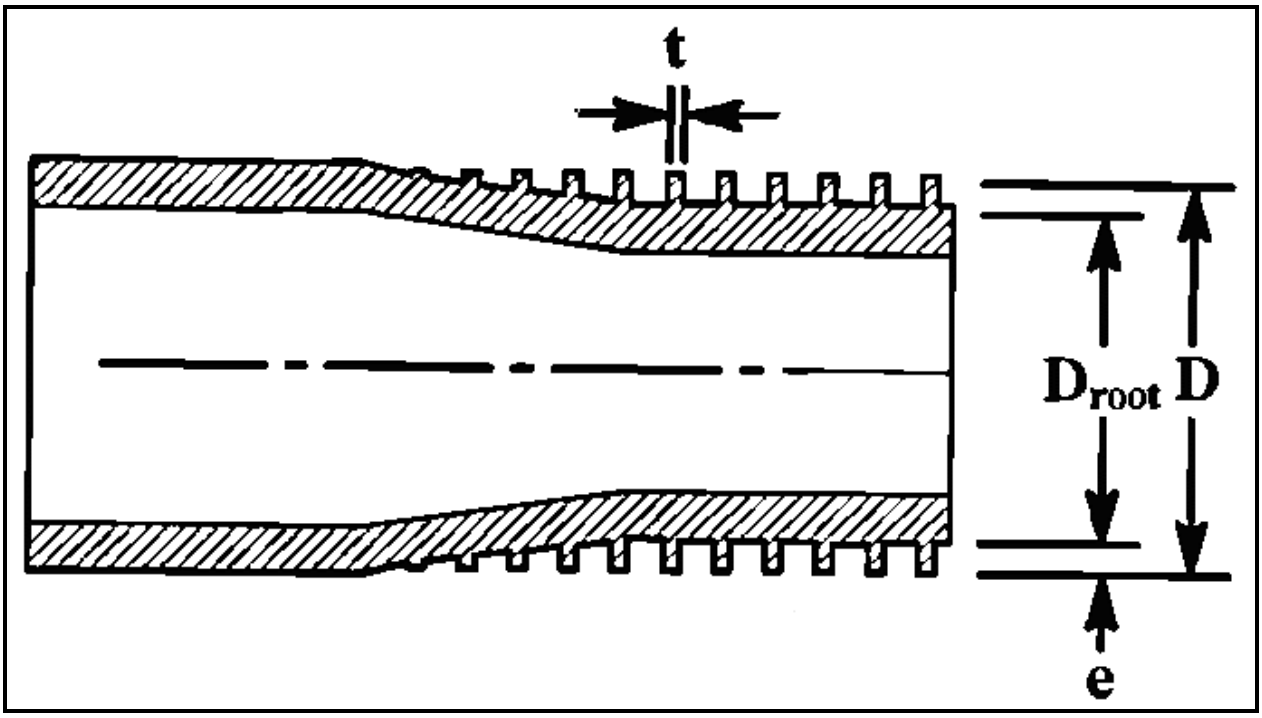

Figure 7.15. Diagram of an integral low finned tube.

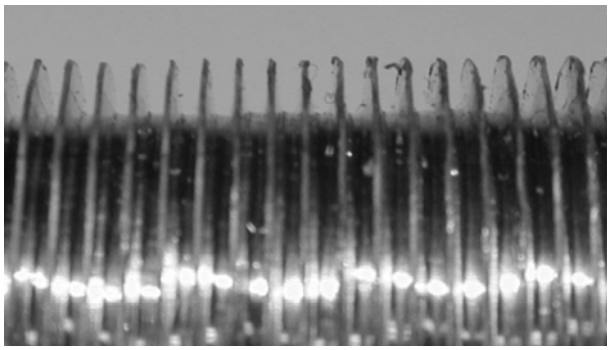

Figure 7.16. Photograph of a low finned tube.

7.7.1 Role of Surface Tension on Film Condensation on Low Finned Tubes

The influence of surface tension on two-phase flow and heat transfer is quite complex. Surface tension itself is a cohesive interfacial force created by the difference between the intermolecular forces at the phase transition interface created by the respective molecules, which are closely packed in a liquid and relatively loosely packed in a vapor. Surface tension is what holds a liquid droplet together and tends to form a geometry that minimizes the interfacial surface area, being it a droplet in a vapor or a small film of liquid on a surface. The pressure difference across a liquid-vapor interface of principal radii r_1 and r_2 is given by the Laplace equation, whose general form is

$$\Delta p = \sigma\left(\frac{1}{r_1}+\frac{1}{r_2}\right) \qquad [7.7.1]$$

where σ is the surface tension and the pressure difference is

$$\Delta p = p_L - p_G \qquad [7.7.2]$$

where p_L is the local liquid pressure and p_G is the local vapor pressure and r is the radius of the interface. For a cylindrical interface, one of the radii goes to infinity and the pressure difference becomes

$$\Delta p = \sigma\left(\frac{1}{r}\right) \qquad [7.7.3]$$

Instead, for a spherical surface the two radii are equal and thus

$$\Delta p = \sigma\left(\frac{2}{r}\right) \qquad [7.7.4]$$

For a constant vapor pressure at isothermal conditions, if the curvature of the interface is not constant, such as for a liquid film on a fin or a corrugation on the surface of a tube, then the local pressure in the liquid will not be constant. This induces flow of the liquid from the region of small curvature towards that with larger curvature. That is, this will create a surface tension driven flow in the film. On the other hand, if the interface is of uniform radius but is subjected to a temperature gradient, again a pressure gradient will be produced in the liquid and cause liquid to flow from the high temperature region (low surface tension) towards the low temperature region (high surface tension). This latter process is referred to as the *Marangoni effect*. This effect is also created if the fluid is a mixture and a concentration gradient exists in the liquid phase along the interface, which creates a surface tension gradient. Of these two surface tension flows, the pressure difference created by curvature of the interface is typically much stronger in film condensation than that of the Marangoni effect for the small temperature differences involved. Hence, condensate flow from the tip of a fin or corrugation towards its base is primarily from the effect of curvature of the liquid-vapor interface.

For condensate formed on a horizontal low fin tube, the two forces acting on the liquid film in quiescent vapor conditions are gravity and surface tension. Here, surface tension draws the liquid from the fin tip towards its root and dominates the gravity force on the liquid with its downward influence. Instead, in the root area between the fins, the radius of the film around the circumference of the tube is relatively large and uniform; thus, gravity dominates in this direction and governs the drainage of condensate from the tube while surface tension tends to promote retention of the condensate between the fins.

The first to exploit this surface tension induced flow in film condensation was Gregorig (1954) and this has become to be known as the *Gregorig effect*, illustrated in Figure 7.17. He proposed a vertical, longitudinally fluted surface on which the condensate is drawn to the troughs by surface tension forces and then drains downward by gravity forces, enhancing heat transfer relative to a planar surface. His work stimulated numerous developments of enhanced condensation surfaces. For more on this topic, refer to the recent review of Shah, Zhou and Tagavi (1999).

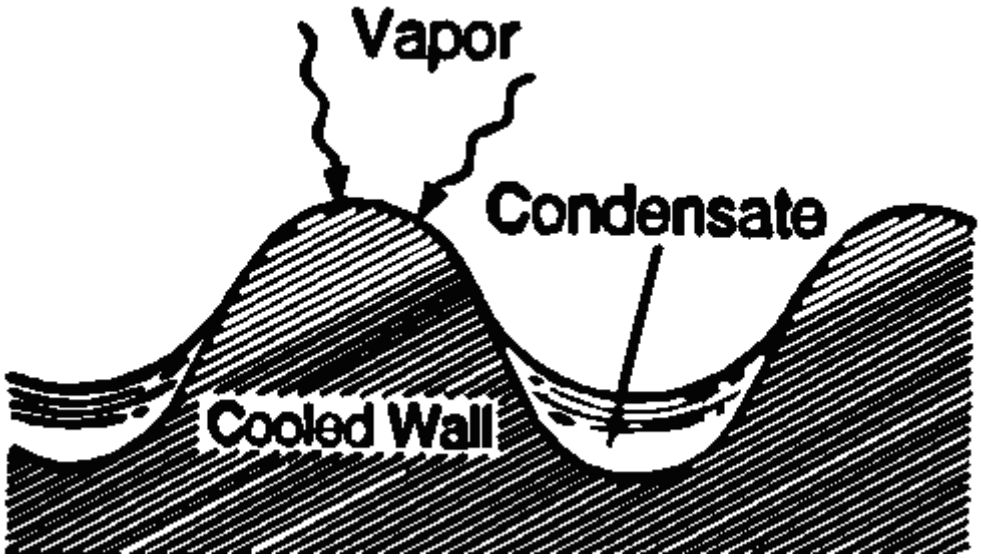

Figure 7.17. Gregorig effect on a liquid film on a fluted surface.

7.7.2 Beatty and Katz (1948) Model of Condensation on a Single Horizontal Low Finned Tube

Beatty and Katz (1948) proposed the first model for condensation heat transfer on a horizontal low finned tube. They applied vertical surface Nusselt analysis to condensation on the fin assuming the condensate drains downwards and Nusselt theory for a horizontal tube to condensation on the root area between adjacent fins i.e. a two-zone approach. The condensation heat transfer coefficient is thus an area weighed average of the condensation coefficient on the root area per unit length A_{root}, referred to as α_{root}, and the condensation coefficient on the fin area per unit length A_{fin} , referred to as α_{fin}. Taking into account the fin efficiency, the condensing coefficient on the low fin tube is

$$\alpha\eta_{surface} = \alpha_{root}\frac{A_{root}}{A_{total}} + \alpha_{fin}\frac{\eta_{fin}A_{fin}}{A_{total}} \qquad [7.7.5]$$

where α is based on the effective external surface area A_{eff} of the low finned tube. The total surface area per unit length A_{total} is

$$A_{total} = A_{root} + A_{fin} \qquad [7.7.6]$$

where A_{fin} includes the fin tip area. The surface efficiency $\eta_{surface}$ is

$$\eta_{surface} = 1 - \frac{A_{fin}}{A_{total}}\left(1 - \eta_{fin}\right) \qquad [7.7.7]$$

The effective external surface area A_{eff} is equal to $\eta_{surface}A_{total}$. The fin efficiency η_{fin} is normally obtained from the fin efficiency expression for a circumferential fin of uniform thickness with an insulated tip, assuming a uniform heat transfer coefficient over its surface. The fin height is corrected for the latter assumption by adding one-half of the fin tip thickness to the height of the fin when calculating the fin

efficiency. Thus, its value can be estimated from the following expression applying the mean heat transfer coefficient on the fin α_{fin}, while also introducing the fouling factor R, as follows:

$$\eta_{fin} = \frac{\tanh\left[m\left(e+\frac{t}{2}\right)\right]}{m\left(e+\frac{t}{2}\right)} \qquad [7.7.8]$$

$$m = \left[\frac{2\left(\frac{1}{\alpha_{fin}}+R\right)^{-1}}{k_{fin}\,t}\right]^{1/2} \qquad [7.7.9]$$

Note that the fouling factor R is often neglected in fin efficiency expressions in textbooks. The fouling factor tends to increase the fin efficiency with increasing values of R, very significantly for tubes of low thermal conductivity. Note that the thermal resistances of the condensing coefficient on the fin and the fouling factor are in series in the above expression since the heat first passes through the condensate film and then through the fouling layer into the fin. In the above expressions e is the fin height, t is the mean fin thickness and k_{fin} is the thermal conductivity of the fin.

For the root area between the fins, the applicable diameter is the root diameter D_{root} at the base of the fins and this diameter is substituted directly into [7.5.7] for condensation on a horizontal plain tube so that

$$\alpha_{root} = 0.725\left[\frac{\rho_L(\rho_L-\rho_G)g\,k_L^3\,h_{LG}}{\mu_L D_{root}(T_{sat}-T_w)}\right]^{1/4} \qquad [7.7.10]$$

The equivalent vertical length is then obtained by taking the surface area for one face of the fin and dividing it by the fin tip diameter D, such that the equivalent length of the fin L_{fin} is

$$L_{fin} = \frac{\pi\left(D^2 - D_{root}^2\right)}{4D} \qquad [7.7.11]$$

Substituting into [7.2.11], the heat transfer coefficient on the side of the fins is

$$\alpha_{fin} = 0.943\left[\frac{\rho_L(\rho_L-\rho_G)g\,k_L^3\,h_{LG}}{\mu_L L_{fin}(T_{sat}-T_w)}\right]^{1/4} \qquad [7.7.12]$$

Thus, one first assumes a wall temperature at the root of the fins and then calculates the respective surface areas and heat transfer coefficients. Then the mean coefficient for the entire tube is obtained. The above equations can be incorporated into one single expression as

$$\alpha\eta_{surface} = 0.689\left[\frac{\rho_L(\rho_L-\rho_G)g\,k_L^3\,h_{LG}}{\mu_L(T_{sat}-T_w)}\right]^{1/4}\left[\frac{A_{root}}{A_{total}}D_{root}^{-0.25} + 1.3\frac{\eta_{fin}A_{fin}}{A_{total}}L_{fin}^{-0.25}\right] \qquad [7.7.13]$$

Beatty and Katz replaced the original value of 0.725 in [7.7.10] with an empirical value of 0.689 that fit their experimental data better for four different fluids they tested. Expression [7.2.19] can be used in place of h_{LG} to include subcooling effects of the condensate. The heat transfer coefficient given by [7.7.13] is defined relative to the effective surface area, i.e. $A_{eff}=A_{root}+\eta_{fin}A_{fin}$. The nominal heat transfer coefficient α_{nom}, based on πDL where L is the length of the tube, is obtained by multiplying α by the ratio of $A_{eff}/\pi DL$, which allows the low finned tube to be compared to a plain tube on a tube replacement basis. Note that their method does not include the effect of condensate retention (see next section) and also the flow on the fins is actually controlled by surface tension and not gravity. Hence their method is reasonably accurate but is unreliable for fluids with large surface tensions or for large fin densities.

7.7.3 Condensate Retention Models for a Horizontal Low Finned Tube

As mentioned above, the Beatty-Katz equation does not account for the condensate retained between the fins on the bottom side of the tube by surface tension forces. The Beatty-Katz approach assumes that all the condensate formed drains off the bottom without any holdup between the fins while a notable perimeter can be affected, typically on the order of 10 to 40% of the circumference. Figure 7.18 depicts the condensate retention half-angle β, which refers to the angle from the bottom of the tube up to the highest point at which condensate is held up to the tip of the fins. Based on a balance of forces, a liquid condensate retention half-angle equation was derived by Honda, Nozu and Mitsumori (1983) as

$$\beta = \cos^{-1}\left\{1-\left(4\sigma\cos\varphi/\rho_L\, g\, b\, D\right)\right\} \qquad [7.7.14]$$

where D is the fin tip diameter and b is the interfin spacing at the fin tips (e.g. fin pitch minus the fin thickness), g is the acceleration due to gravity and σ is the surface tension. φ is one-half the apex angle of the fin in *radians* (typically about 3-7° for standard trapezoidal low fins and 0° for a rectangular fin).

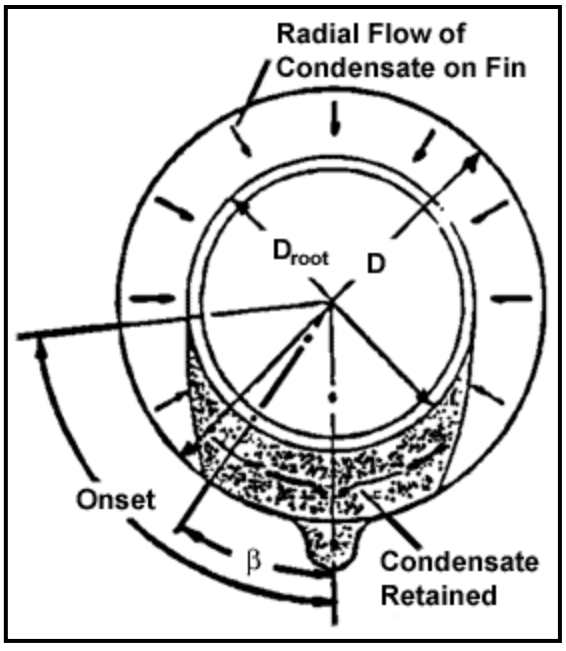

Figure 7.18. Condensate retention angle on a low fin tube.

Rudy and Webb (1985) subsequently observed experimentally the retention angle on a variety of low finned tubes and arrived at the following expression for the half-angle of the tube that retains condensate:

$$\beta = \cos^{-1}\left\{1-\left[\frac{2\sigma\left[\left(2e/\cos\varphi\right)+t_{tip}-t_{root}\right]}{D\rho_L\, g\,(s\, e-A_{p)}}\right]\right\} \qquad [7.7.15]$$

In the above expression, the half-angle β is in radians, e is the fin height, t_{tip} is the fin thickness at the tip, t_{root} is the fin thickness at the root, s is the fin pitch, A_p is the cross-sectional area of the fin, and φ is one-half the apex angle of the fin in radians. The expression worked quite well for their measured retention angles. These two expressions give the same retention angle for rectangular fins. For trapezoidal fins, they also give the same result if b is set to the mean interfin spacing. They are applicable when e > b/2; note also that when $(\sigma\cos\varphi)/(\rho_L gbD) > 0.5$ the interfin space is fully flooded and β should be set to π.

7.7.4 Webb, Rudy and Kedzierski (1985) Model of Condensation on a Single Horizontal Low Finned Tube

Utilizing their condensate retention equation, Webb, Rudy and Kedzierski (1985) improved on the Beatty-Katz model to obtain

$$\alpha\eta_{surface} = (1-c_b)\left[\alpha_{root}\frac{A_{root}}{A_{total}} + \eta_{fin}\,\alpha_{fin}\frac{A_{fin}}{A_{total}}\right] + c_b\,\alpha_b \qquad [7.7.16]$$

Here α_{fin} is determined from surface tension driven flow on the fins as

$$\alpha_{fin} = 0.943\left[\frac{\rho_L\, k_L^3\, h_{LG}}{\mu_L(T_{sat}-T_w)}\right]^{1/4}\left[\frac{2\sigma}{e^2}\left(\frac{1}{s}+\frac{1}{t}\right)\right]^{1/4} \qquad [7.7.17]$$

and α_{root} is determined based on gravity controlled flow as

$$\alpha_{root} = 1.514\left[\frac{\mu_L^2\, Re_{root}}{g k_L^3 \rho_L^2}\right]^{-1/3} \qquad [7.7.18]$$

where the film Reynolds number of the condensate flowing in the root area is

$$Re_{root} = \frac{4\Gamma_{root}}{\mu_L(s-t_{root})} \qquad [7.7.19]$$

Γ_{root} is obtained from

$$\Gamma_{root} = \Gamma_{fin} + \left[\alpha_{root} A_{root}(T_{sat}-T_w)/h_{LG}\right] \qquad [7.7.20]$$

and

$$\Gamma_{fin} = \alpha_{fin}\eta_{fin}A_{fin}(1-c_b)(T_{sat}-T_w)/h_{LG} \qquad [7.7.21]$$

The condensate flooded fraction of the tube perimeter c_b is equal to β/π while the unflooded fraction completely available for film condensation is $(1\text{-}c_b)$. They also included the heat transfer on the flooded perimeter of the tube α_b, estimating its value numerically. However, it is simpler to assume laminar, fully developed flow in a rectangular channel of the same width but twice the fin height (to represent the interfin half-channelas a closed channel) and thus allows textbook solutions based on aspect ratio to be applied to calculate the Nusselt number for the laminar flow heat transfer to obtain α_b.

7.7.5 Other Recent Low Finned Tube Condensation Models

More complex theoretical models for condensation on two-dimensional low finned tubes have been developed, such as those of Adamek (1981), Honda and Nozu (1986), and Adamek and Webb (1990). For a more detailed review, refer to Webb (1994) or Shah, Zhou and Tagavi (1999). On the other hand, Rose (1994) proposed a simplified empirical approach that captures most of the features of these analytical models and also predicts a large independent experimental database covering steam, glycol, hydrocarbons

and refrigerants. Furthermore, the method of Rose is able to predict the optimum fin spacing for the fluid in question, which is particularly important when choosing the best available fin density for an application, and the method is still relatively simple to implement. Thus, this method is described below.

Rose (1994) began by defining a condensing enhancement ratio $\varepsilon_{\Delta T}$ for low finned and smooth tubes operating at the same condensing temperature difference ΔT (i.e. the saturation temperature minus the base wall temperature) as:

$$\varepsilon_{\Delta T} = \frac{\alpha \text{ of finned tube}}{\alpha \text{ of smooth tube}} = \frac{(q/\Delta T) \text{of finned tube}}{(q/\Delta T) \text{of smooth tube}} = \frac{q \text{ of finned tube}}{q \text{ of smooth tube}} \qquad [7.7.22]$$

The enhancement ratio at the same heat flux q on each tube ε_q is instead defined as:

$$\varepsilon_q = \frac{\alpha \text{ of finned tube}}{\alpha \text{ of smooth tube}} = \frac{(q/\Delta T) \text{of finned tube}}{(q/\Delta T) \text{of smooth tube}} = \frac{\Delta T \text{ of finned tube}}{\Delta T \text{ of smooth tube}} \qquad [7.7.23]$$

In the above expressions, the heat flux q and heat transfer coefficient α are based on the same smooth tube surface area, determined with the diameter D for the smooth tube and the root diameter D_{root} for the finned tube, respectively. Hence, to convert the low finned tube heat transfer coefficient from its nominal surface area at D_{root} in this method to its nominal surface area value at the fin tip diameter D, the former value must be multiplied by the ratio D/D_{root}. Since q is typically found to be nearly proportional to $\Delta T^{4/3}$ for both smooth and low finned tubes according to Rose, $\varepsilon_{\Delta T}$ and ε_q are therefore related as follows:

$$\varepsilon_q = (\varepsilon_{\Delta T})^{4/3} \qquad [7.7.24]$$

This means that the enhancement ratio is higher when comparing a low finned tube to a smooth tube at the same heat flux than when making the comparison at the same condensing temperature difference. The general enhancement expression of Rose (1994) for a low finned tube for $\varepsilon_{\Delta T}$ is:

$$\varepsilon_{\Delta T} = \left(\frac{D}{D_{root}}\right)\left(\frac{t_{tip}}{b + t_{tip}}\right) T_t + \frac{\pi - \beta}{\pi}\left(\frac{1 - F_f}{\cos\varphi}\right)\left(\frac{D^2 - D_{root}^2}{2D_{root}(b + t_{tip})}\right) T_f + \frac{\pi - \beta}{\pi}(1 - F_s) B_l \left(\frac{s - t_{root}}{b + t_{tip}}\right) T_s \qquad [7.7.25]$$

In this expression, the first term to the right gives the fin tip enhancement effect, the second term gives that relative to the sides of the fin and the last term gives that regarding the root area between adjacent fins. The thickness of the fin at the tip is t_{tip}, the thickness of the fin at its root is t_{root}, the interfin spacing between the flanks of two adjacent fins at their tip is b, the fin pitch is s, the condensate retention angle from the *bottom* of the tube is β and one-half of the apex angle of the fin itself is φ (equal to the angle between the flank of the fin and its vertical axis). The term $(\pi-\beta)/\pi$ in the above expression is equivalent to $(1-c_b)$ in the method of Webb, Rudy and Kedzierski (1985) described earlier. Expression [7.7.14] is used by Rose to calculate β. This expression is applicable when $\beta \leq \pi$; at $\beta = \pi$ only the fin tips contribute to film condensation heat transfer and the other two terms for the fin flanks and interfin root area are neglected when calculating for smaller fin spacings, which produces a sharp inversion in the value of $\varepsilon_{\Delta T}$ when simulating the effect of interfin spacing with the other geometrical parameters fixed. The other parameters in his method are determined as described below.

In the above expression, F_f and F_s are the fractions of the flank areas of the fins and the interfin root area influenced by the liquid retention due to capillary forces at the base of sharp-edged fin roots on the upper part of the tube above the fully flooded zone of the tube perimeter, i.e. the condensate retained as wedges at the roots of the fins in the "unflooded" zone of the tube which reduce heat transfer performance. For trapezoidal fins with sharp-edged fin roots from the analysis of Masuda and Rose (1987), these fractions for the fin flanks and the root area between fins are calculated respectively as:

$$F_f = \left(\frac{1-\tan(\varphi/2)}{1+\tan(\varphi/2)}\right)\left(\frac{2\sigma\cos\varphi}{\rho_L g D_{root} e}\right)\left(\frac{\tan((\pi-\beta)/2)}{\pi-\beta}\right) \qquad [7.7.26a]$$

$$F_s = \left(\frac{1-\tan(\varphi/2)}{1+\tan(\varphi/2)}\right)\left(\frac{4\sigma}{\rho_L g D_{root}(s-t_{root})}\right)\left(\frac{\tan((\pi-\beta)/2)}{\pi-\beta}\right) \qquad [7.7.26b]$$

Owing to some approximations in the derivations of these two parameters, they sometimes marginally exceed unity in value and in that case the relevant parameter is reset to unity. For rectangular fins, this expression is simplified with $\varphi = 0$. For specially configured fins with a fin root radius such that an inscribed arc touches both the fin flanks and the interfin root surface at the root diameter, no condensate is retained above the angle β and thus F_f and F_s are zero according to Masuda and Rose (1987). Refer to Rose (1994) for further details.

Continuing with the description of the Rose (1994) method, the parameters T_t, T_f and T_s are determined as follows:

$$T_t = \left\{\frac{D_{root}}{D} + \frac{B_t G_t}{0.728^4}\right\}^{1/4} \qquad [7.7.27a]$$

$$T_f = \left\{\left(\frac{0.943}{0.728}\right)^4 \frac{D_{root}}{e_{eff}} + \frac{B_f G_f}{0.728^4}\right\}^{1/4} \qquad [7.7.27b]$$

$$T_s = \left\{\frac{(\xi(\pi-\beta))^3}{0.728^4} + \frac{B_s G_s}{0.728^4}\right\}^{1/4} \qquad [7.7.27c]$$

The effective vertical fin height is used in [7.7.27b], where $e_{eff} = e(\pi-\beta)/\sin(\pi-\beta)$ when $(\pi-\beta) \le \pi/2$ whereas $e_{eff} = e(\pi-\beta)/(2-\sin(\pi-\beta))$ when $\pi \ge (\pi-\beta) \ge \pi/2$. In [7.7.27c], the function $\xi(\pi-\beta)$ is determined from the following polynomial fit to the integration of the condensate film thickness in the Nusselt theory to the angle $(\pi-\beta)$ to simplify the method's implementation:

$$\xi(\pi-\beta) = 0.874 + 0.001991(\pi-\beta) - 0.02642(\pi-\beta)^2 + 0.005530(\pi-\beta)^3 - 0.001363(\pi-\beta)^4 \qquad [7.7.28]$$

The parameters G_t, G_f and G_s are determined as:

$$G_t = \frac{\sigma D_{root}}{(\rho_L - \rho_G) g t_{tip}^3} \qquad [7.7.29a]$$

$$G_f = \frac{\sigma D_{root}}{(\rho_L - \rho_G) g e^3} \qquad [7.7.29b]$$

$$G_s = \frac{\sigma D_{root}}{(\rho_L - \rho_G) g (s - t_{root})^3} \qquad [7.7.29c]$$

The empirical constants found by matching this method to his database yielded $B_t = B_f = B_s = 0.143$ and $B_1 = 2.96$. It predicted his database to a standard deviation of 12.4% and also predicted the trends correctly for fin density (interfin spacing) for three different fluids. To account for the effect of fin efficiency, which is particularly important for tube materials with thermal conductivities lower than copper, Briggs and Rose (2004) have provided a simple iterative method to account for the influences on the fin tip and fin flank heat transfer.

7.7.6 Effects of Tube Row and Vapor Shear on Low Finned Tube Arrays

Low finned tubes promote the Helmholz-Kelvin instability in the condensate flowing off the bottom of the tube such that the column mode is encouraged as shown in Figure 7.19. The low fins also inhibit lateral spreading of the impinging film along the lower tube and the majority of the condensate flows around a low finned tube with minimal lateral spreading. As a consequence, large zones of the finned surface between these columns are unaffected by condensate from the tubes above and hence these zones function as if they were in the top row. Therefore, applying the Nusselt and Kern tube row factors, in [7.6.5] and [7.6.7], to low finned tube bundles is extremely conservative, resulting in significant under-predicting of the bundle's condensing heat transfer coefficient. Some experimental studies found tube row exponents as low as -1/25 but it is more prudent value to use a tube row exponent of -1/10 or -1/12.

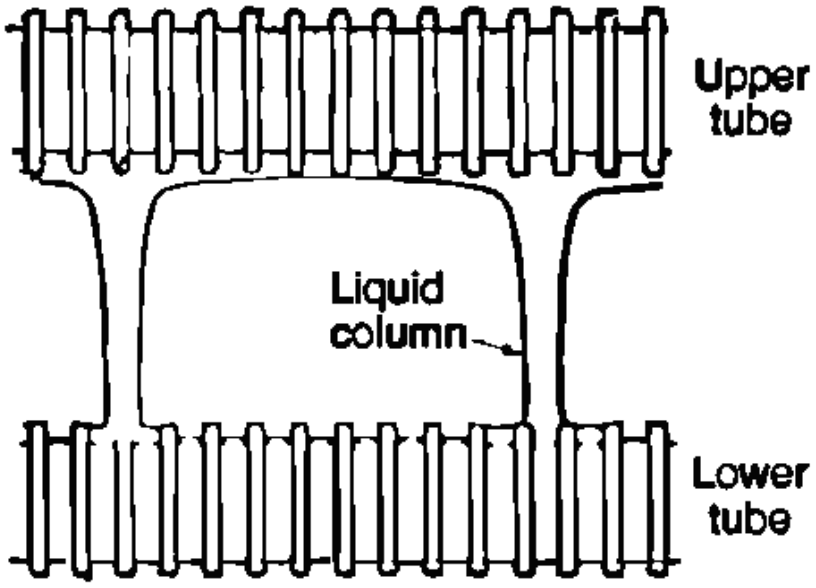

Figure 7.19. Condensate flow as a column jet between low finned tubes.

Furthermore, in the recent study of Gstöhl and Thome (2006a) for R-134a condensing at 30°C on a Wolverine 26 fpi Turbo-Chil tube array of ten tubes, very small tube row effects were found for film Reynolds numbers reaching up to 4250 for vertical tube pitches of 25.5, 28.6 and 44.5 mm for their 18.94 mm fin tip diameter tubes at three levels of nominal heat flux. Their results are shown in Figure 7.20 for

which tube row exponents ranged from -1/14 to -1/100. Based on all their data, the mean tube row exponent was found to be -1/33. Thus for thermal design, a prudent value of -1/25 may be the best choice but certainly applying the value -1/6 proposed by Kern (1958) for plain tubes to low finned tubes is too conservative and needlessly penalizes the application of low finned tubes.

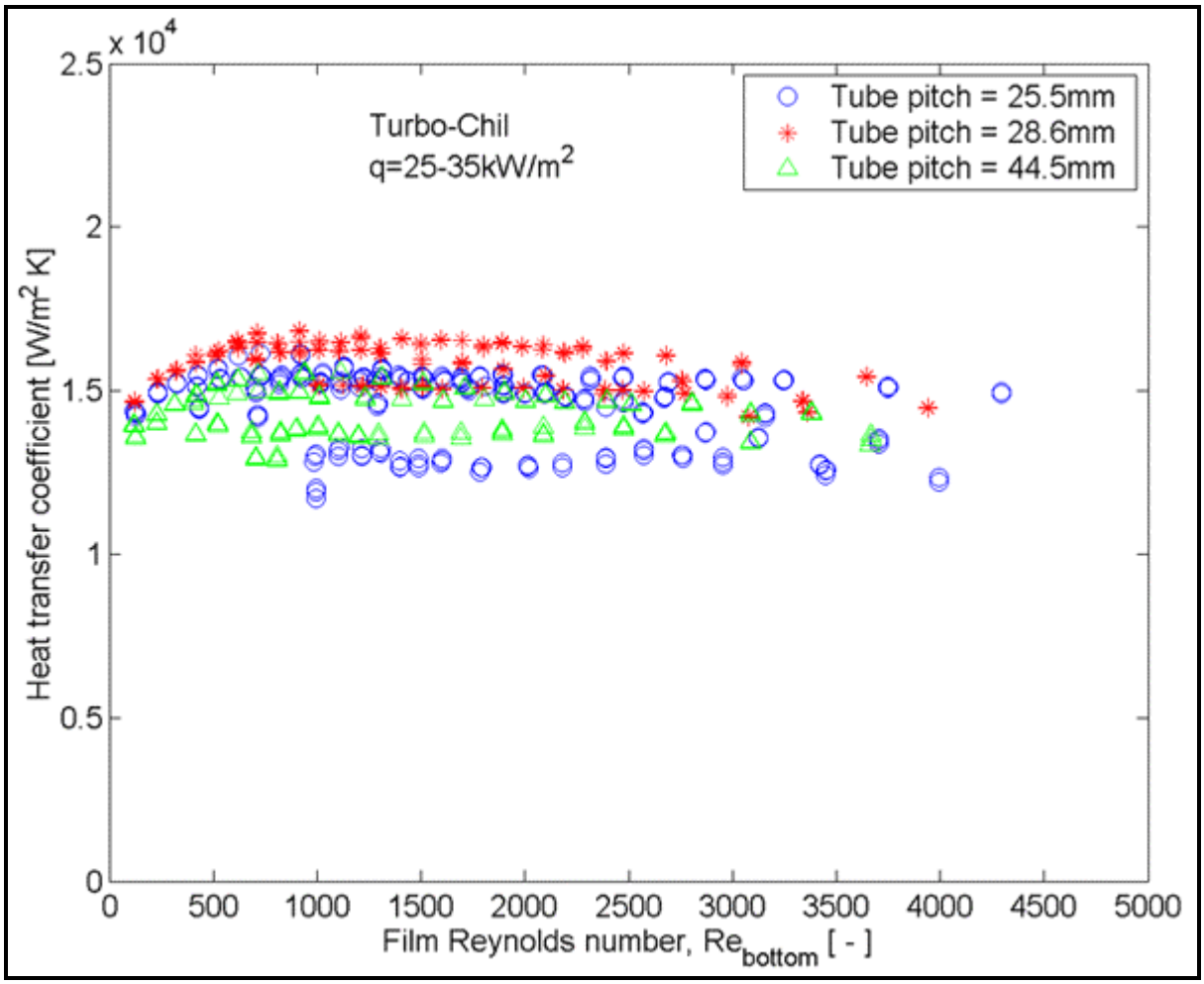

Figure 7.20. Condensation data for Turbo-Chil low finned tube array of Gstöhl and Thome (2006a).

In order to illustrate the dynamics of the condensate flow on a low finned tube array, Figure 7.21 from Gstöhl and Thome (2006c) shows a time sequence taken during condensation without liquid overfeed at a nominal heat flux of 40 kW/m^2. First, three "temporary" columns are formed below the top tube. When they impinge on the second tube, the liquid columns do not spread axially along the tube but instead the condensate is channeled by the fins to flow around the tube. Then the diameters of these columns decrease and they break down. The liquid that impinged on the second tube flows around the tubes and leaves at the bottom at the same axial positions. The three columns formed below the second tube are twisted and exist for about the same period as the "temporary" columns formed below the first tube. If one interprets this in terms of the tube row effect, it is clear that the lower tubes in this array of low finned tubes have only a limited part of their length inundated by condensate from above while most of the length suffers no inundation *and* this process occurs only intermittently so that for some periods of time there is *no* inundation at all, thus explaining the very small tube row exponent for low finned tubes.

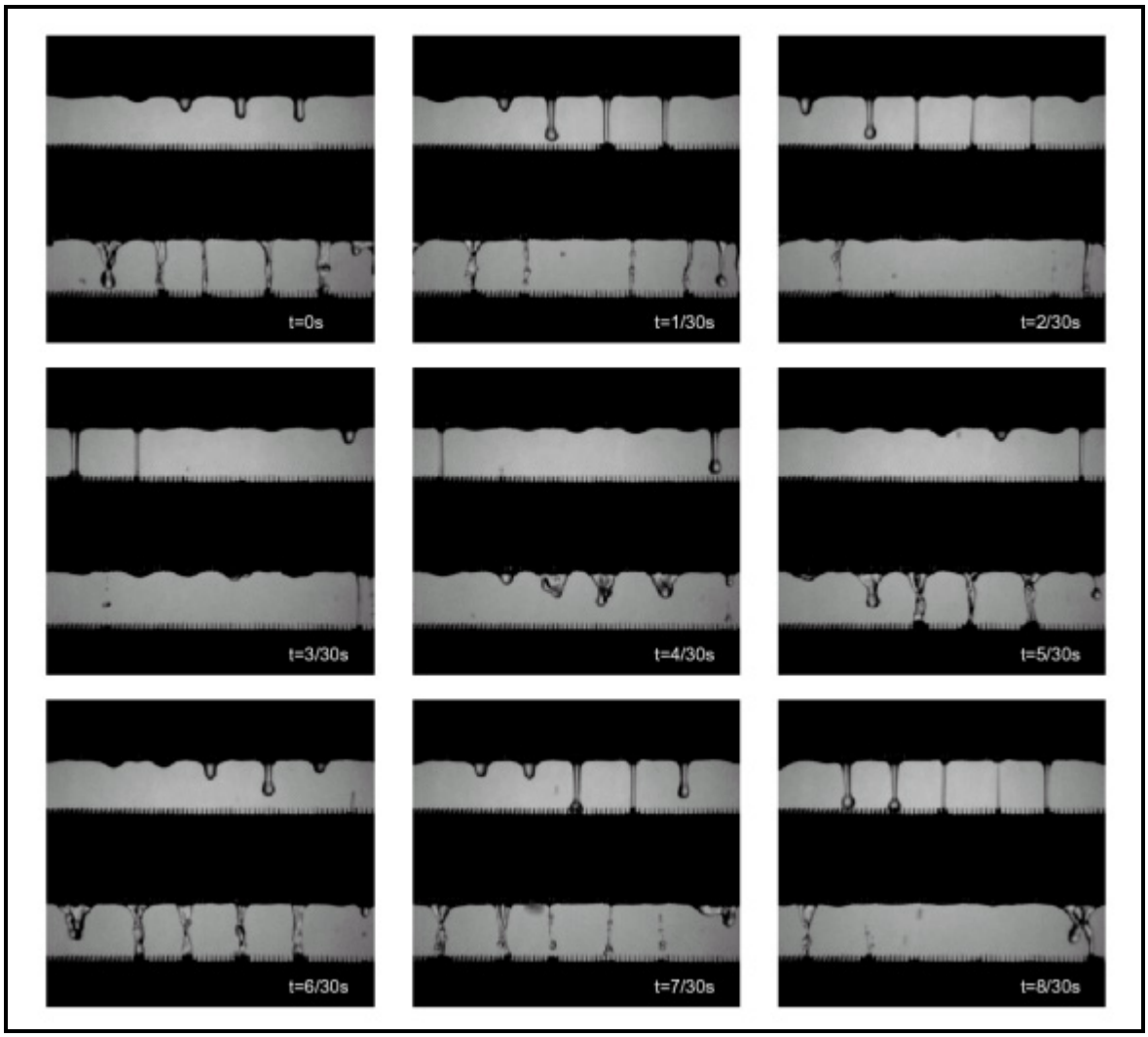

Figure 7.21. Time sequence of condensate flow on the second tube in an array of low finned tubes at a tube pitch of 28.6 mm for R-134a condensing at a nominal heat flux of 40 kW/m^2 from Gstöhl and Thome (2006c).

Cavallini et al. (1995) investigated the effect of interfacial vapor shear on condensation on a single low finned tube. According to their experiments, a very large vapor Reynolds number threshold must be surpassed before a significant influence is seen on low finned tube performance. Videos described in Cavallini et al. (1994), with several exemplary photographs, also prove that the vapor shear has little effect on the condensate retention angle, at least up to the point where the condensate is then literally blown off the tube and a mist flow is formed. Thus, low finned tube bundles can be designed using only a single-tube condensation model together with the appropriate tube row equation, as long as the film flow remains in the laminar regime and the vapor Reynolds number remains below 100,000.

Cavallini et al. (1996) proposed an asymptotic method for the combined effect of gravity and vapor shear on a single-tube:

$$\alpha = \left(\alpha_{sv}^2 + \alpha_{fc}^2\right)^{1/2} \qquad [7.7.30]$$

where α_{sv} is the heat transfer coefficient on the finned tube under stationary vapor conditions and α_{fc} is the heat transfer coefficient under forced convection (vapor shear controlled) conditions.

$$\alpha_{fc} = C_{fc}\left(\frac{k_L}{D}\right)Re_{eq}^{0.8}\,Pr_L^{1/3} \qquad [7.7.31]$$

and the empircal lead constant is determined from

$$C_{fc} = 0.03 + 0.116\left(t_{tip}/s\right) + 0.07\left(e/s\right) \qquad [7.7.32]$$

Re_{eq} is the equivalent Reynolds number and Pr_L is the liquid Prandtl number. To extend this method to tube bundles, α_{sv} could be obtained by applying the tube row correction using an exponent of -1/10 or -1/12 or even to -1/25 based on recent results from the single tube row study by Gstöhl and Thome (2006a) mentioned above.

7.7.7 Three-dimensional Enhanced Condensing Tubes

Integral low finned tubes with three-dimensional fins are made by notching of conventional two-dimensional low fins to form saw-toothed fins, or by crosscutting the fins. This greatly reduces condensate retention and enhances heat transfer coefficients on the fins. While several comprehensive experimental studies have been published for these tubes, no general analytical method is available at this time for predicting their performance. Several experimental studies are described below.

Briggs, Yang and Rose (1995) completed a very accurate, comprehensive experimental comparison of 17 commercially available low finned tube geometries, including both 2-d trapezoidal fins and notched 3-d fins, for R-113. One 2-d trapezoidal fin gave the same performance as the best of the 3-d notched fins, but the 3-d fins had not been optimized for use with R-113.

Rewert, Huber and Pate (1996a, 1996b) measured condensing coefficients for R-123 and R-134a in a comparison of a 1024 fpm (26 fpi) low finned tube, a 1575 fpm (40 fpi) low finned tube, a Turbo-CII tube and a Gewa-SC tube (the latter have 3-d enhancements). The Turbo-CII tube significantly outperformed the 40 fpi low finned tube (the better of the two low fin tubes) while the Gewa-SC only provided moderate improvement with respect to the 40 fpi tube. In tests on a five-by-five staggered tube bundle and using liquid overfeed to simulate up to 30 tube rows, they reported data by tube row for these fluids and tubes. Figure 7.22 depicts four graphs of performance. For both fluids, the Turbo-CII shows a faster falloff in tube row performance than the other tubes; since it starts from a much larger top tube row value, its overall condensing performance is still higher than the other tubes, however. The tube row effect of the Gewa-SC tube in the lower left graph is nearly negligible, with the lower tubes performing like the top tube.

Chen and Tuzla (1996) ran extensive tests on a 19 mm (3/4 in.) Turbo-CII of Wolverine Tube at a saturation temperature of 37.7°C (100°F) for R-22, R-134a, R-410a and several zeotropic refrigerant mixtures. The R-134a performance was slightly above that of R-22 while R-410a outperformed those fluids by about 15%. Performances of the zeotropic mixtures were much lower as they suffered from the mass diffusion resistance in the vapor phase.

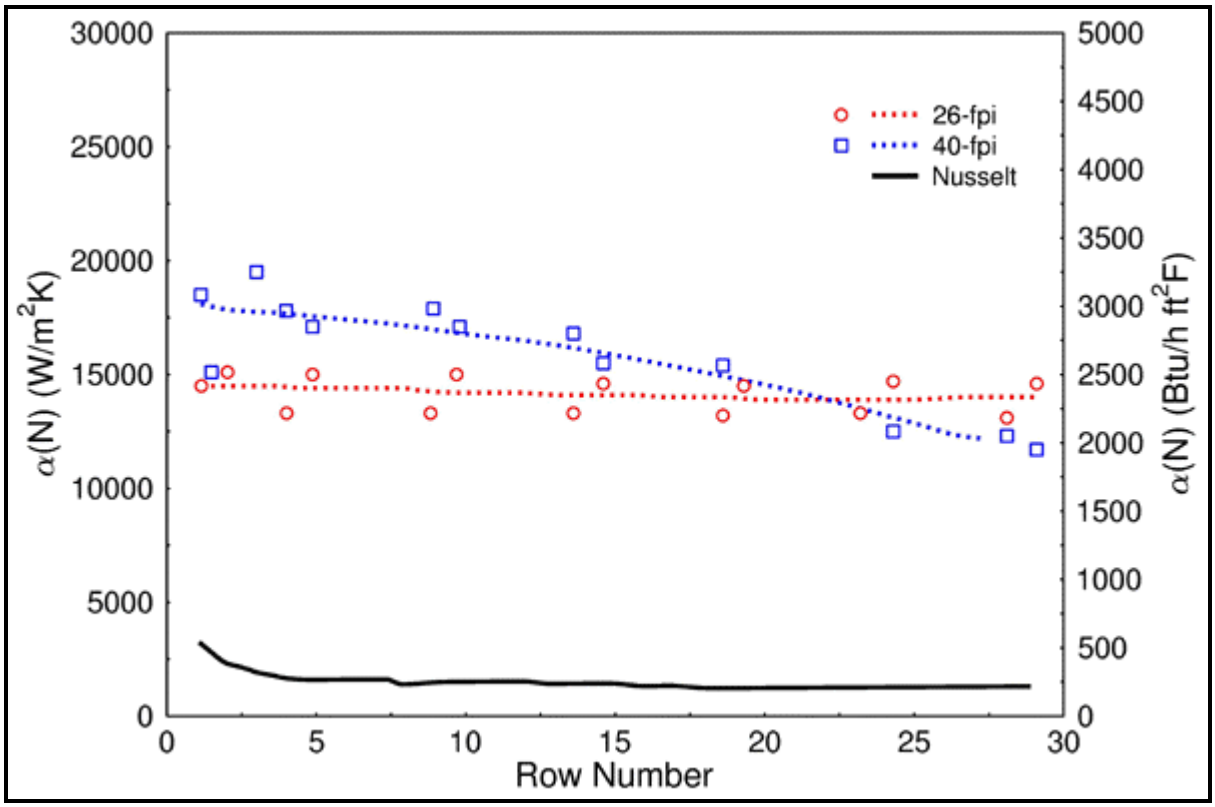

Fig. 7.22 (a): low finned tubes with R-134a.

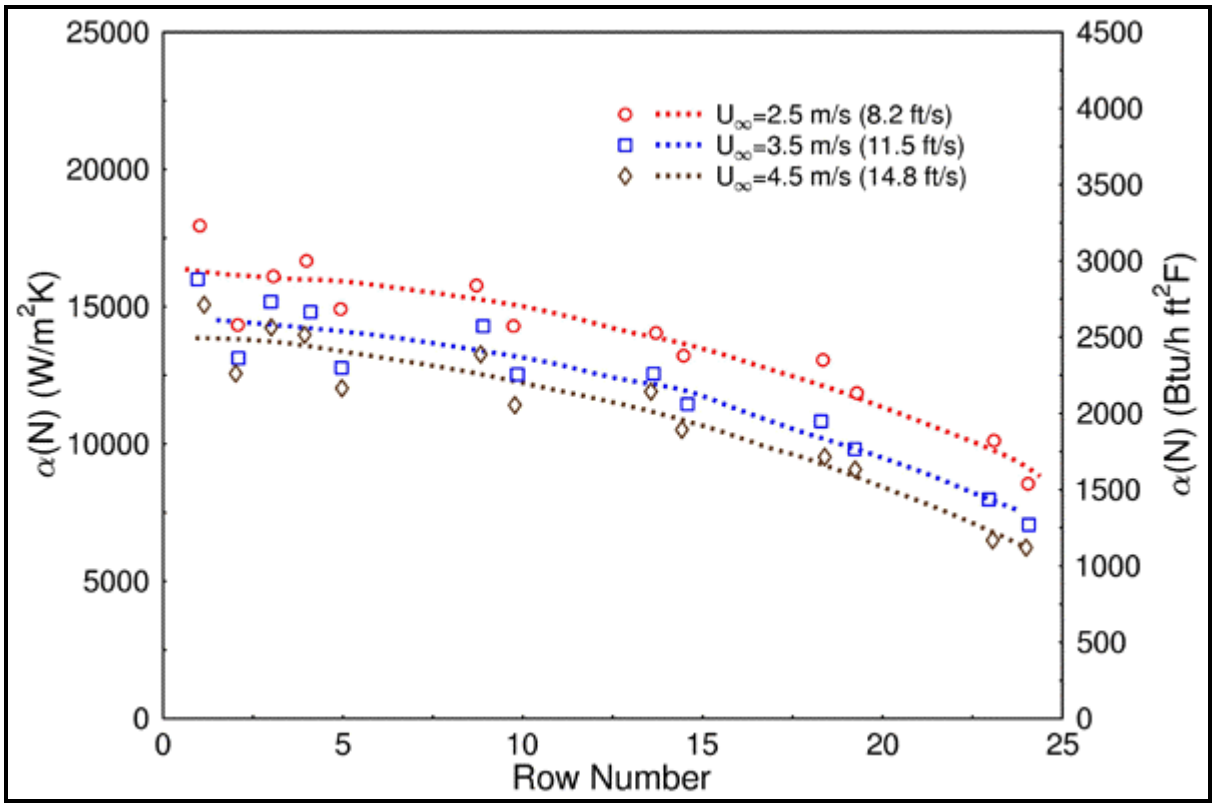

Fig. 7.22 (b): 40-fpi tube with R-123.

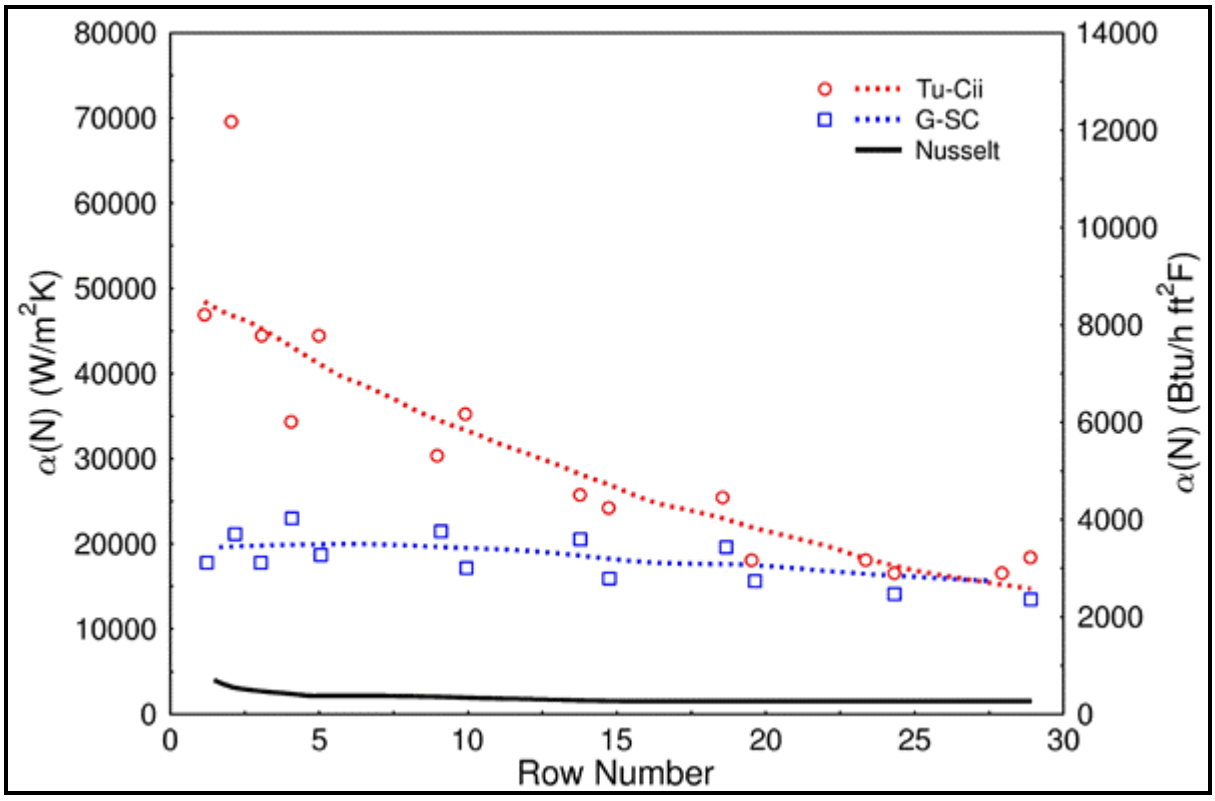

Fig. 7.22 (c): Turbo-Cii and G-SC for R-134a.

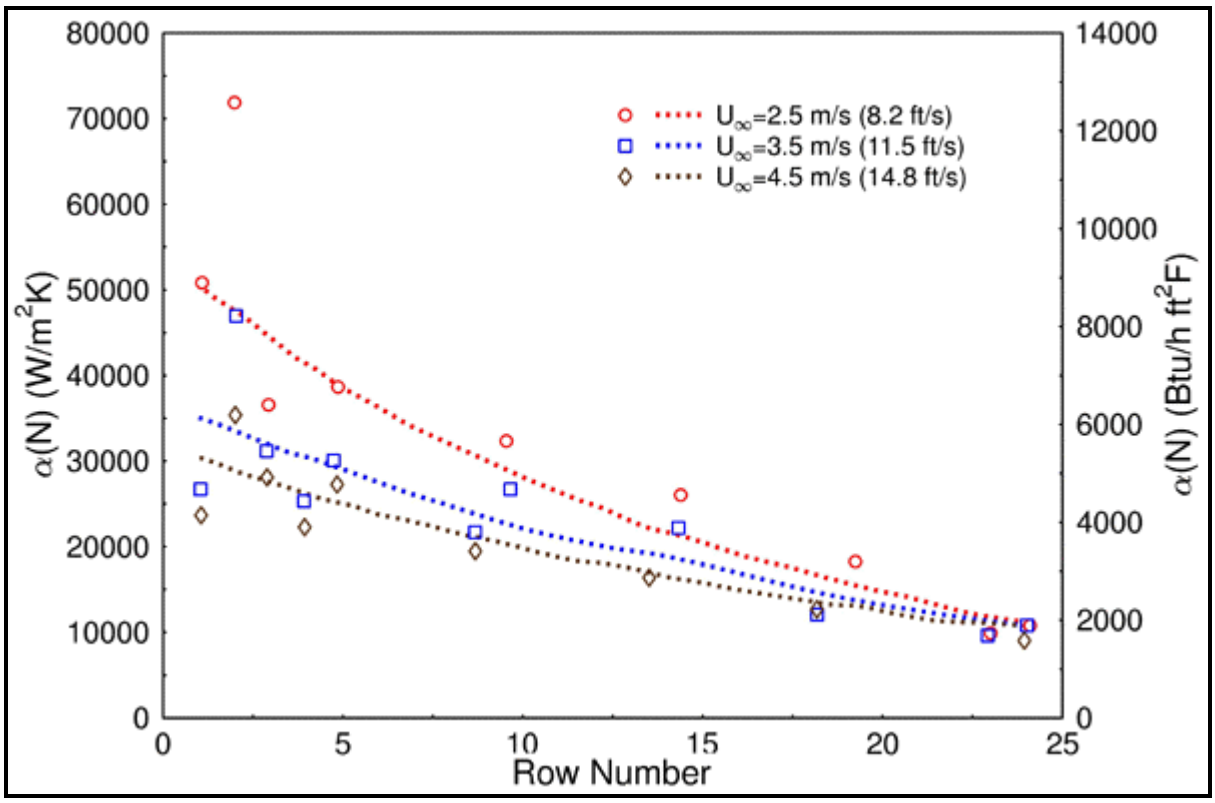

Fig. 7.22 (d): Turbo-Cii for R-123.

Figure 7.22. Condensing data of Rewerts, Huber and Pate (1996a, 1996b). (a): low finned tubes with R-134a; (b): 40 fpi tube with R-123; (c): Turbo-Cii and G-SC for R-134a; (d): Turbo-Cii for R-123. [their figs. 4 & 8 and 4 & 5 reprinted by permission of ASHRAE Trans., 1996 copyright by American Society of Heating, Refrigeration and Air-Conditioning Engineers]. [Note: these figures are shown on the two previous pages.]

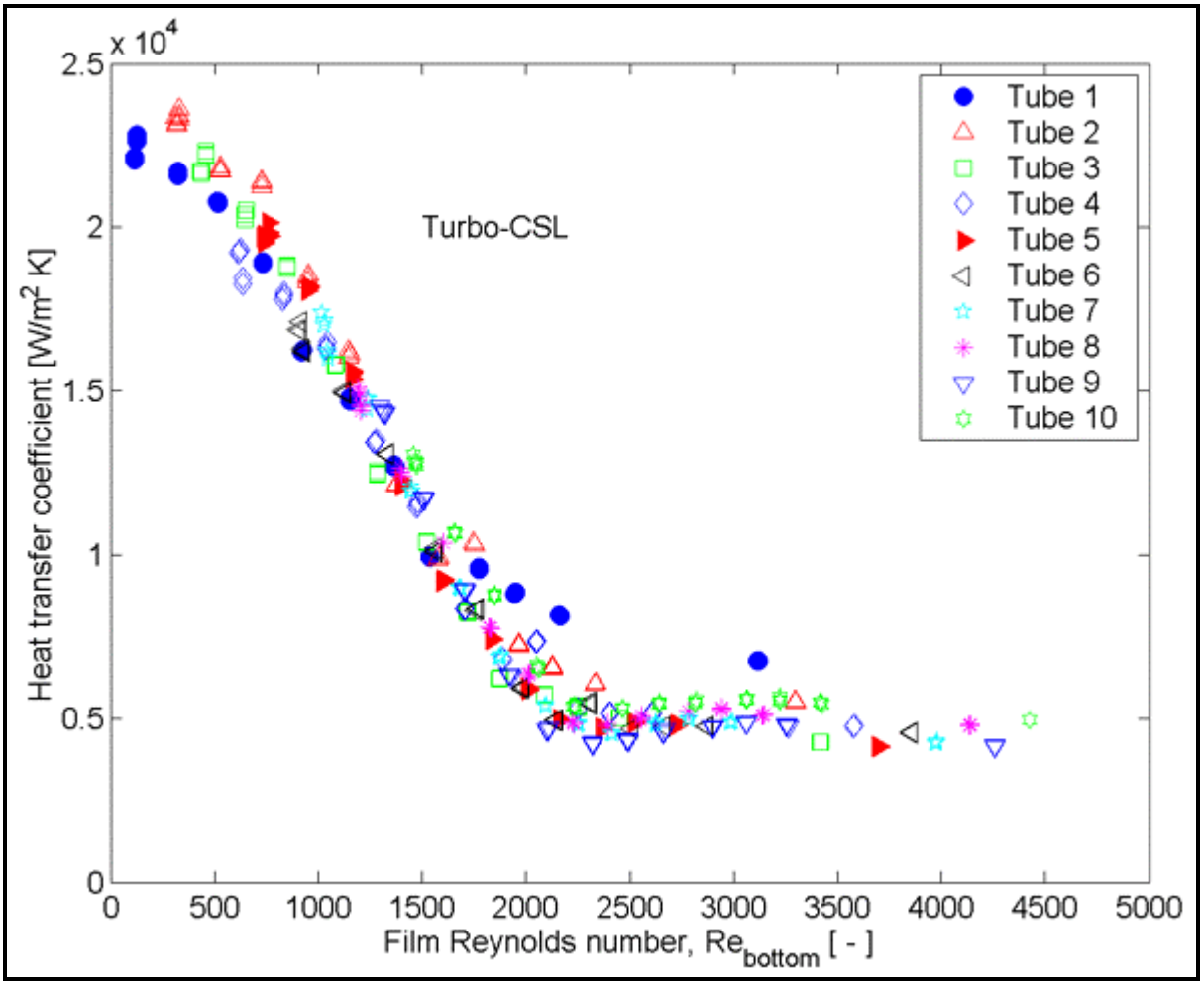

Figure 7.23. Heat transfer measurements with liquid inundation on the Turbo-CSL tube with a tube pitch of 25.5 mm at a nominal heat flux of 40 kW/m^2 from Gstöhl and Thome (2006a).

Gstöhl and Thome (2006a, 2006b, 2006c) performed a study on film condensation of R-134a at a saturation temperature of 30°C for horizontal tube arrays with tube rows numbering from 6 to 10 Wolverine Turbo-CSL enhanced condensation tubes, obtaining both heat transfer measurements and flow visualizations. The results of one series of tests with liquid overfeed are shown in Figure 7.23 for an array of 10 Turbo-CSL tubes. The heat transfer coefficient is plotted versus the film Reynolds number of the condensate leaving the bottom of each tube. These measurements were performed with a tube pitch of 25.5 mm at a mean nominal heat flux of 40 kW/m^2. Starting with no liquid overfeed (Γ=0 kg/ms), the mass flow rate was increased in 12 steps to a maximum mass flow rate of Γ=0.135 kg/ms. The film Reynolds numbers were determined from an energy balance with the assumption that all the liquid condensed on a tube flows onto the tube below. The film Reynolds number is the local value at the midpoint of the tube where the local heat transfer coefficient is determined. Different symbols are used

for the ten tubes to illustrate the evolution of heat transfer performance of every tube as the liquid inundation rate is increased. Without overfeed (lowest film Reynolds number datapoint for each symbol), the heat transfer coefficient decreases from a value of about 23 kW/m^{2}K on the first tube to a value of about 13 kW/m^{2}K on the tenth tube in the array. In general, the heat transfer coefficient is high at low film Reynolds numbers and it decreases with increasing film Reynolds number. At a film Reynolds number of about 2200, the heat transfer coefficient reaches a plateau and flattens out. This trend is observed on all ten tubes in the array proving the consistency of the experimental setup with overfeed to simulate a large number of tube rows where only the top tube deviates a little from the others. At low film Reynolds numbers, its heat transfer coefficients are a little below the other tubes and at high film Reynolds numbers its values are higher than the other tubes. This might be explained by the fact that the liquid flow leaving the distribution half tube above the top tube differs from the liquid flow leaving from the bottom of an enhanced tube. The film Reynolds number leaving the tenth tube during the measurement with the highest inundation rate would correspond approximately to the 30th row in a heat exchanger at this heat flux.

During each series of measurements, the nominal row heat flux was held constant, but the experimental setup had five cooling water inlet flows for the 10 tube rows, so that each two rows of tubes constituted two tube passes. Thus, the heat flux varied substantially between the even and odd rows and, as seen in Figure 7.23, the heat transfer coefficients are higher on the upper tubes in the array as the inundation is less. These two effects lead to the following range of heat fluxes for the data at a nominal heat flux of 40 kW/m^2 with an overfeed rate of Γ=0.027 kg/ms, starting at the top tube to the tenth tube: 36, 57, 35, 49, 33, 44, 30, 38, 26 and 36 kW/m^2. In fact, about half the scatter of the data points in the figure is due to this difference in heat flux, which is not differentiated in their graph.

Figure 7.24 depicts the heat transfer coefficients measured on a Turbo-CSL tube row as a function of the film Reynolds number for all three tube pitches tested: 25.5, 28.6 and 44.5 mm. For clarity, only the data in the heat flux range from 25 to 35 kW/m^2 are shown to partly eliminate the effect of heat flux. It can be seen that for all three tube pitches the heat transfer coefficient decreases with increasing film Reynolds number and flattens out at a certain film Reynolds number due to the liquid slinging effect. The larger the tube pitch the earlier this happens, and thus the higher the plateau in the heat transfer coefficient. At the tube pitch of 44.5 mm typical of a staggered tube layout in a condenser, the plateau is reached at Re_{bottom} = 1100 and this gives a higher condensing heat transfer performance than that of the Turbo-Chil low finned tube presented earlier in this chapter for similar test conditions which had little tube row effect.

Below, the enhanced tube prediction method for the Turbo-CSL tube proposed by Gstöhl and Thome (2006b) is presented based on their results for one refrigerant (R-134a), at one saturation temperature (30°C), one tube row and the three tube pitches mentioned above. While the method is not general, it can be fit to future data sets for other test conditions, to other tubes and to other fluids to simulate the performance of enhanced tube condensers (albeit without including the effects of nearby tube rows or vapor shear, a topic of current study with the same test facility).

As their first step in correlating the heat transfer behavior of the Turbo-CSL tube, only the measurements without condensate slinging were considered (the data before the plateau). Furthermore, during laminar film condensation, the heat transfer coefficient is dependent on the condensation temperature difference and consequently applying Newton's concept of a heat transfer coefficient defined as the ratio of heat flux to the temperature difference (saturation temperature minus base wall temperature) is debatable in such a case, as pointed out for instance by Rose (2004). In other words, for calculating the heat flux for a given temperature difference, the heat transfer coefficient is multiplied by the temperature difference. When the heat transfer coefficient itself depends on the temperature difference (as is the case here), nothing is gained by separating the correlation for calculating the heat flux into a heat transfer coefficient and a condensation temperature difference.

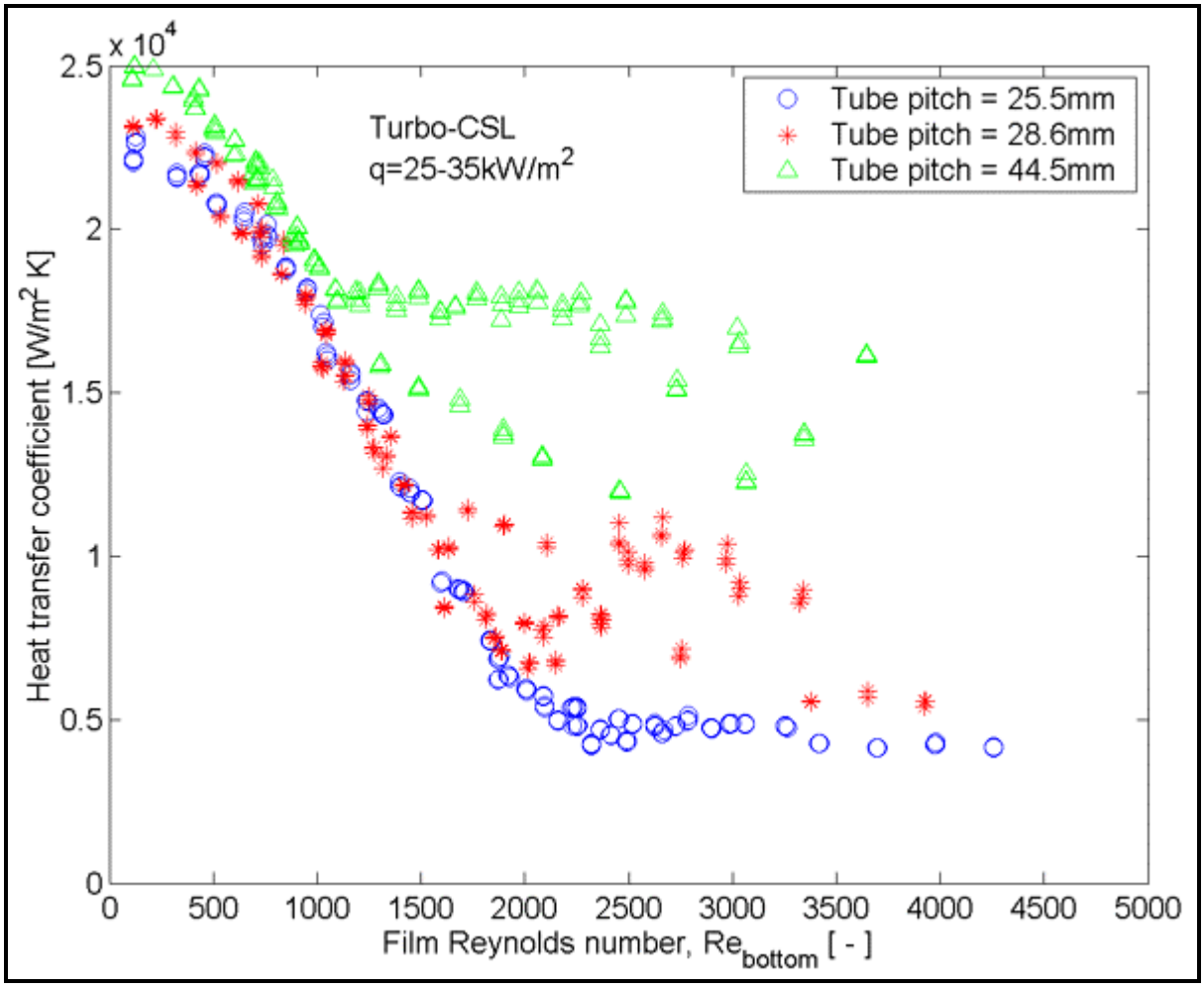

Figure 7.24. Tube spacing influence of the Turbo-CSL tube at a nominal heat flux of 40 kW/m^2 over a limited heat flux range from Gstöhl and Thome (2006a) illustrating the three plateaus at the three tube pitches created by liquid slinging.

From a fundamental point of view, it is helpful to look at the local heat flux as a function of the condensation temperature difference since integrating the local heat fluxes in a tube bundle gives its overall heat duty. During the measurements, the heat flux decreases with increasing liquid inundation for the same condensation temperature difference. For the Turbo-CSL tube, the analysis was performed for film Reynolds numbers equal to 0 up to 2000 where the condensate starts to get slung off the tube array. Applying the above logic, the following dimensional equation was proposed by Gstöhl and Thome (2006b) to describe the performance of the Turbo-CSL enhanced tube:

$$q = \left(a + c\,Re_{top,N}\right)\Delta T^{b} \qquad [7.7.33]$$

The heat flux q is that for the nominal surface area at the tip of the enhancement while ΔT is T_{sat} - T_{wall} where the wall temperature is that at the root of the enhancement, for the Nth tube row. The empirical values of a, b and c for the Turbo-CSL were found to be 25350 W/m^2, 0.89 and -9.4 W/m^2, respectively. The standard deviation gives a measure of how the relative errors are distributed around the mean relative

error. Assuming a Gaussian distribution of relative errors, 68% would be within ± σ and 95% within ± 2σ. The mean relative error for the Turbo-CSL tube is –1.0% with a standard deviation of 9.3%.

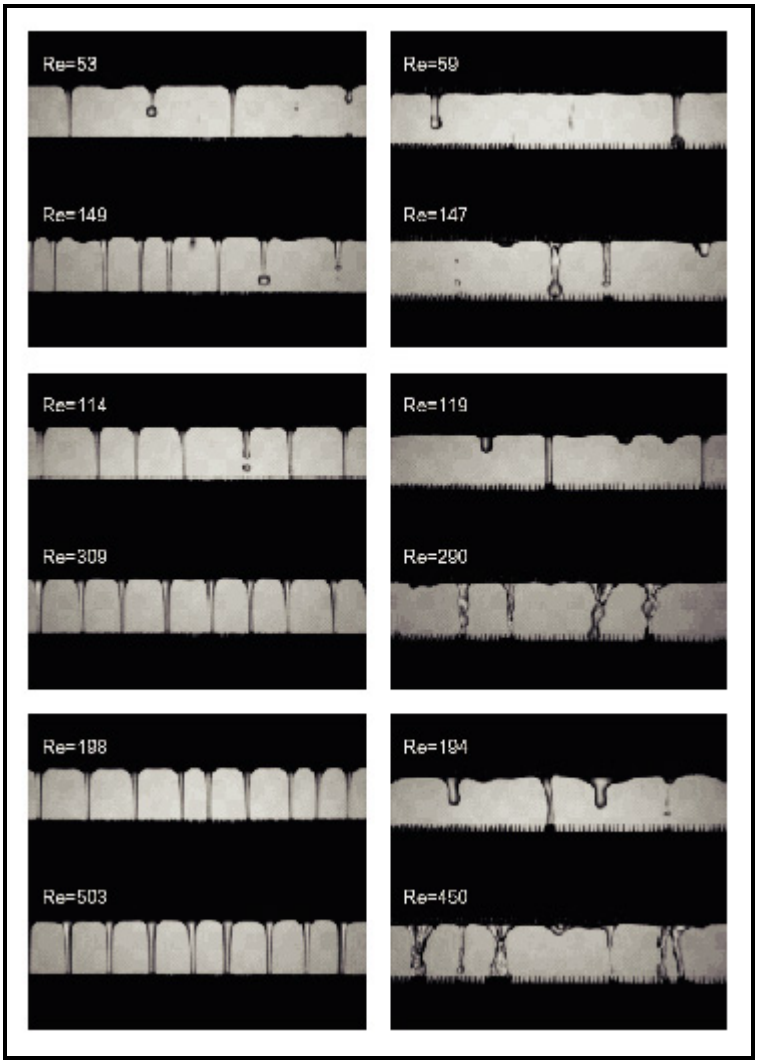

Figure 7.25. Intertube flow patterns observed on the second tube in the array (without overfeed) at a tube pitch of 28.6 mm for R-134a condensing at a nominal heat flux of 20 kW/m^2 (top row), 40 kW/m^2 (middle row), and 60 kW/m^2 (bottom row): Turbo-CSL (left column) and Turbo-Chil (right column).

During their visualizations reported in Gstöhl and Thome (2006c), instabilities in the condensate flow between tubes were observed. Figure 7.25 illustrates some images on this process for the Turbo-CSL tube and similar images for the Turbo-Chil low finned tube. For the 3D enhanced tube, the instabilities occurred near the transition to sheet mode or within the sheet mode. At the transition, a continuous sheet was temporarily formed and then when it broke down, some condensate left the array of tubes sideways without contacting the lower tubes. This break down phenomenon was less frequent when the film Reynolds number was increased as the sheet became more continuous. However, the continuous sheet was always unstable, moving a little forward and backward with respect to the vertical axis of the array. For a further increase in film Reynolds number, this unstable movement was amplified and regular

oscillations with frequencies of about 1.5 Hz were observed. At high film Reynolds numbers, the amplitude became so large that a significant fraction of the condensate left the tubes sideways (the amount of which however was not able to be measured experimentally). This phenomenon was regular and it appeared that the amount of liquid leaving the array of tubes on the front was the same as that leaving on the back, indicating that this was not caused by imperfections of the experimental setup. As seen before, heat transfer deteriorates with increasing inundation. When some of the condensate is slung off the array, the tubes below receive less condensate at their top than otherwise expected, which has a beneficial effect on their heat transfer coefficients.

For this reason, a realistic heat transfer model must account for the fraction of condensate leaving the tube row sideways in the sheet mode. In an ideal situation, the condensate flows in a continuous sheet from the bottom of one tube onto the top of the tube below as in Figure 7.26 (left). The actual condensate does not however fall vertically in a stable sheet, but instead, it oscillates back and forth (and front and back), as depicted in Figure 7.26 (middle). With increasing mass flow rate, the amplitude of oscillation increases and the condensate leaves the bottom of the tube at a sufficiently large angle relative to the vertical that some liquid misses the tube below. This maximal angle of deflection varies in time and is denominated θ_{def}. It was assumed that θ_{def} is a function of the film Reynolds number based on their visual observations. The critical angle θ_{crit} is the angle that delineates contact with the next tube row as illustrated in Figure 7.26 (right). As long as $\theta_{def} < \theta_{crit}$, the condensate sheet oscillates on the top of the lower tube, but all the condensate remains on the tube but when $\theta_{def} > \theta_{crit}$, a fraction of the condensate misses the lower tube. The critical angle θ_{crit} depends on the geometry of the tube array according to equation [7.6.22].

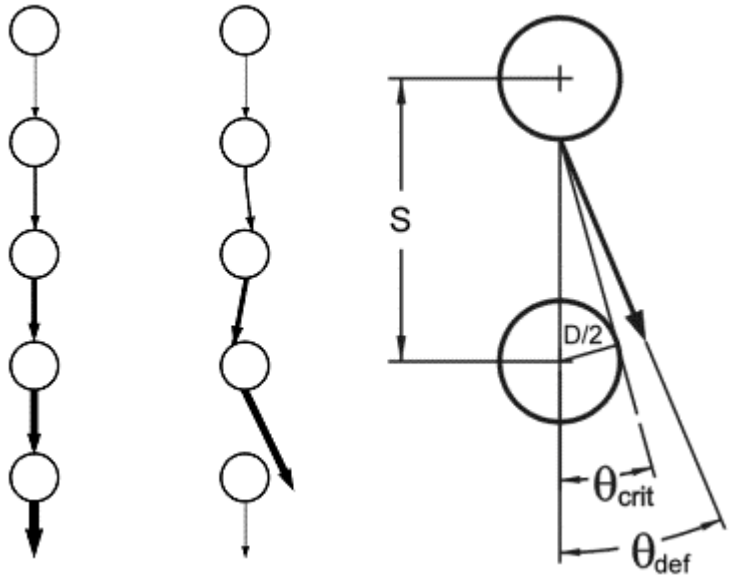

Figure 7.26. Ideal flow (left), liquid "slinging" (middle) and critical slinging angle (right).

The fraction of condensate that misses the lower tube is assumed to be proportional to the ratio $(\theta_{def}-\theta_{crit})/\theta_{def}$. This means that the film Reynolds number on the top of the nth tube in the array can be expressed as

$$\mathrm{Re}_{\mathrm{top,n}} = \frac{\theta_{\mathrm{crit}}}{\theta_{\mathrm{def}}}\mathrm{Re}_{\mathrm{bottom,N-1}} \qquad [7.7.34]$$

Once the actual amount of condensate that falls on the top of the tube is known, the expression [7.7.33] can be used to determine the heat flux on the particular tube, starting from the top tube row and working down. As long as no condensate leaves ($\theta_{def} < \theta_{crit}$ so that $Re_{bottom,N-1} = Re_{top,N}$), equation [7.7.33] is used to determine the heat flux on the tube and then by an energy balance gives the amount of condensate leaving the bottom of the tube. As soon as part of the condensate starts to leave (when $\theta_{def} > \theta_{crit}$), equation [7.7.34] is used to determine the amount of condensate that arrives on the tube below and subsequently [7.7.33] is used to determine the heat flux on the tube. The relationship between the angle θ_{def} and the film Reynolds number was assumed to be a linear function as follows:

$$\theta_{def} = d\, Re_{bottom,N-1} + e \qquad [7.7.34]$$

The empirical constant d was found to be 0.00027 radians and e equal to 0.08 radians for this enhanced tube. Nearly as good a fit was found by setting e to zero and using d = 0.00031 radians. Thus, the Reynolds number of the condensate coming off the bottom of the upper tube $Re_{bottom,N-1}$ is used to predict the Reynolds number of the condensate reaching the top of the next tube $Re_{top,N}$ when $\theta_{def} > \theta_{crit}$.

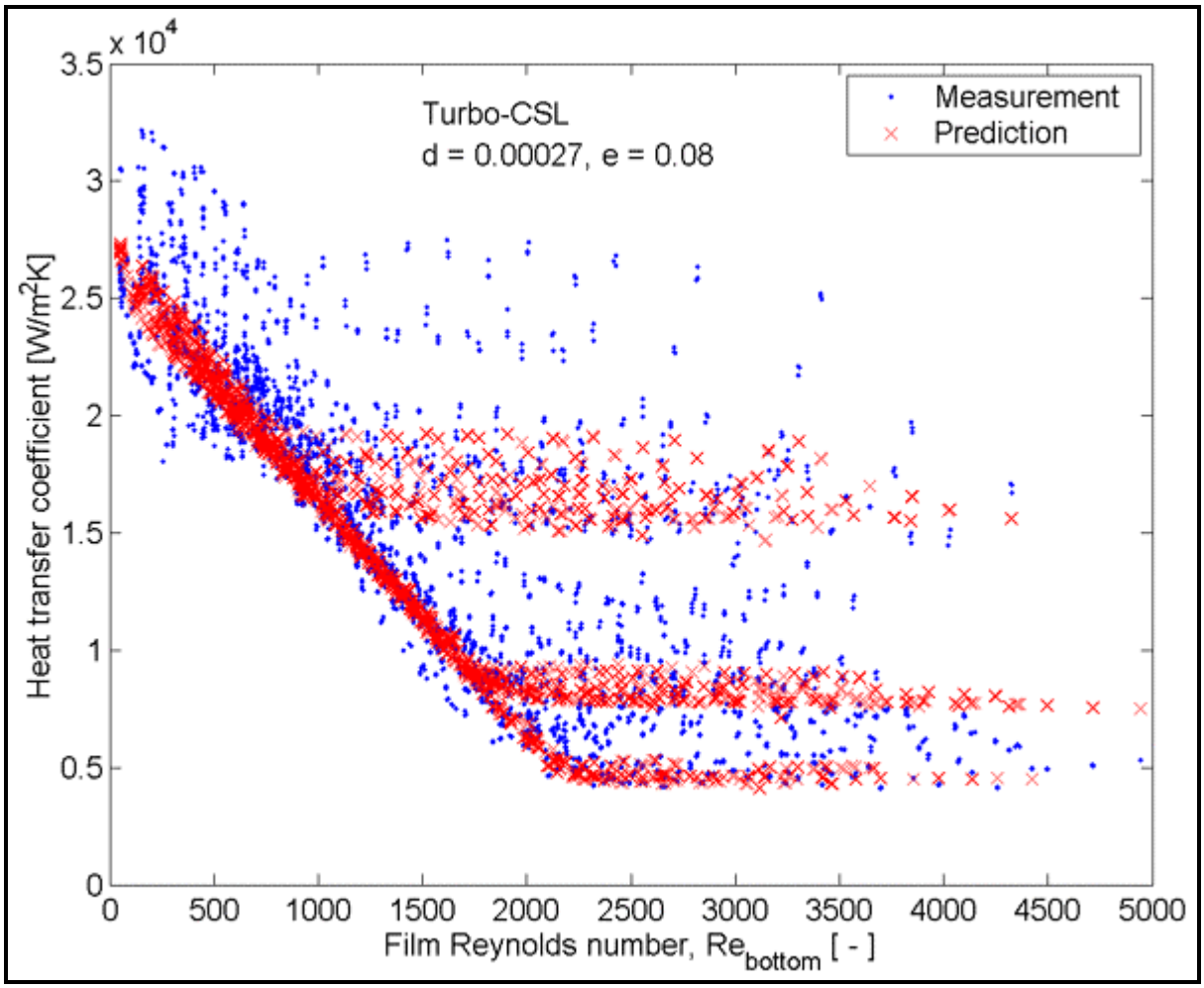

Figure 7.27. Comparison of predictions to measurements for Turbo-CSL tubes from Gstöhl and Thome (2006b), capturing the three slinging levels for the three tube pitches.

Figure 7.27 shows a comparison of the measured and predicted heat transfer coefficients for all measurements for the Turbo-CSL enhanced tube row data. The predicted heat transfer coefficient flattens out at three different levels corresponding to the three tube pitches (and hence three different values of θ_{crit}). For these points in the plateau, the amount of liquid condensed on the tube must be nearly equal to the amount of liquid that is slung off. The values of θ_{crit} for the three tube pitches tested here were 36°, 30° and 16°. The "plateaus" in the predicted heat transfer coefficients for the three different tube pitches can be seen and interpret the associated data quite well. Each level of the plateau corresponds to a certain percentage of condensate leaving the array of tubes sideways. The plateau observed at the smallest tube pitch of 25.5 mm (the lowest plateau) corresponds approximately to 3% of the condensate leaving the array sideways. At the largest tube pitch of 44.5 mm, approximately 10% of the condensate does not fall on the tube below and leaves the array of tubes sideways. The method fit the database including those with the slinging effect to a mean relative error of -3% with a standard deviation of 13%.

7.8 Condensation with Non-Condensable Gases

Condensation in the presence of a non-condensable gas occurs in numerous heat exchanger applications. The most common example is dehumidification in an air-conditioning system, in which water vapor is partially condensed out as the humid air passes through the evaporator. Another prime example is shell-side condensation in surface condensers used in central power plants. Here, a small fraction of air that is dissolved in the feedwater and it eventually arrives at the condenser together with the steam, where of course it cannot condense. Hence, it will build up its concentration near the exit region of the condenser if it is not removed with a steam ejector or some other similar device. In chemical processing plants and refineries, non-condensable gases may be present in the process vapor leaving a distillation column that goes to the overhead condenser or be produced in a reactor prior to a feed effluent heater. A non-condensable gas creates a significant mass transfer resistance to heat transfer depending on the circumstances.

Figure 7.28 depicts this process in the presence of air under quiescent conditions. The total pressure of the bulk vapor-air mixture is p while partial pressures of the vapor (G) and non-condensable gas (a) are $p_{G\infty}$ and $p_{a\infty}$, respectively. The bulk concentrations of vapor and air are $W_{G\infty}$ and $W_{a\infty}$, respectively (note that $W_G + W_a = 1$ at any location). $T_{G\infty}$ is the bulk temperature of the vapor-air mixture and T_w is the wall temperature where T_w is less than the dew point temperature of the vapor. As heat is transferred from the vapor-air mixture to the cold wall, a condensate layer is formed on the wall and then condensation proceeds at the interface (denoted by the subscript i). The non-condensable gas arriving at the interface does not condense and, assuming it is not absorbed by the condensate (typically only a small fraction is), its local concentration builds up at the interface to W_{ai}. Since $W_{Gi} = 1 - W_{ai}$, then the local concentration of the vapor at the interface is W_{Gi}. This reduces the partial pressure of the vapor at the interface to p_{Gi} and the saturation temperature at the interface is T_{Gi}. Condensation of the vapor at the interface creates a mass diffusion process and its associated mass diffusion layer where the non-condensable gas diffuses away from the interface towards the bulk where its concentration is lower. The vapor arrives at the interface by (i) bulk motion of the vapor towards the interface (where it is removed as condensate) and (ii) by mass diffusion down its concentration gradient from the bulk to the interface.

The thermal resistances encountered by the process are thus *three* rather than *one* for condensation of a pure vapor. First of all, there is the thermal resistance across the condensate film itself, whose value is determined using a pure vapor heat transfer expression for the cold wall (plate or tube) where the film may be laminar, laminar-wavy or turbulent. Then there is either natural convection heat transfer or forced convective heat transfer across the temperature gradient from $T_{G\infty}$ to T_{Gi}, depending on whether there is forced flow of the gas-vapor mixture or not. Finally, there exists a mass transfer resistance to the diffusion

of vapor to the interface. Depending on the local circumstances, one or two of these resistances may be negligible with respect to the others.

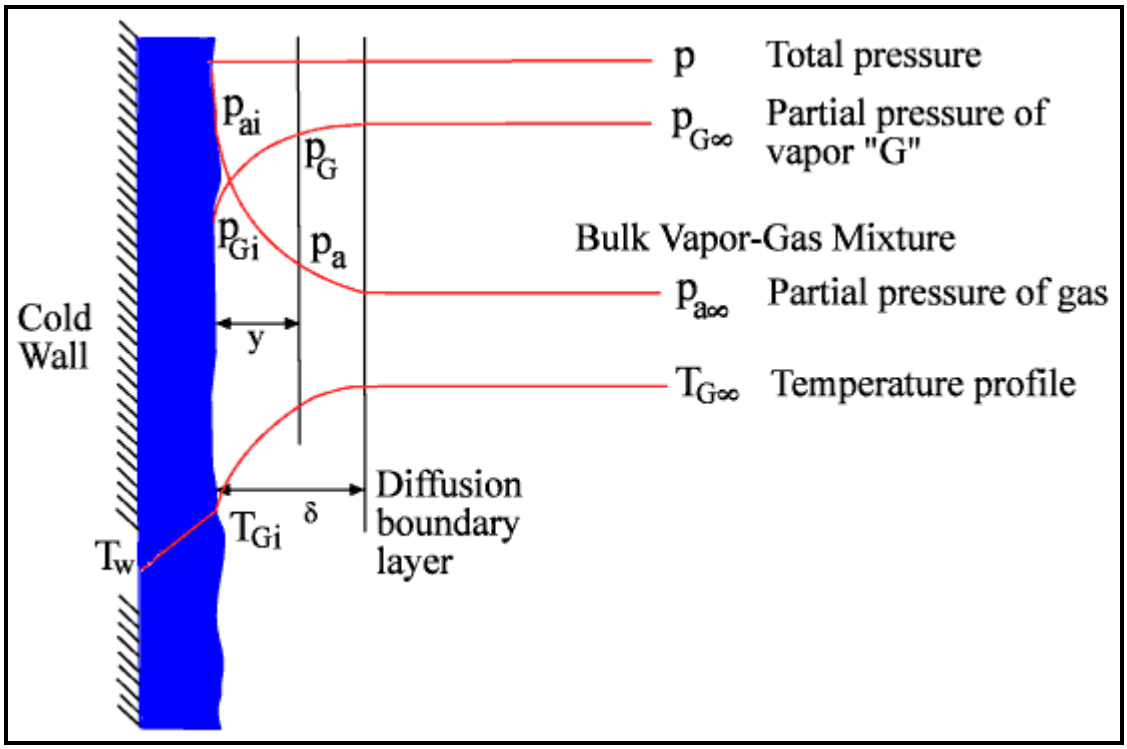

Figure 7.28. Condensation in the presence of a non-condensable gas.

Various boundary layer treatments of condensation with non-condensable gases have been presented in the literature over the years. For example, Minkowycz and Sparrow (1966) analyzed this process for stagnant vapor conditions while Sparrow, Minkowycz and Saddy (1967) studied forced convention conditions. Figure 7.29 depicts the effect of small fractions of air in saturated steam for falling film condensation under stagnant and forced convection conditions. The vertical axis shows the condensing heat flux with air present relative to that of pure steam for otherwise identical conditions, e.g. the ratio is equal to 1.0 for no air present. For quiescent vapor conditions, even a small fraction of air reduces thermal performance significantly. For forced convection conditions, the fall in thermal performance is less but is still of particular magnitude. This comparison shows the importance of attaining high flow rates of the vapor-air mixture to minimize the mass diffusion resistance. A simpler approach by Colburn is described in Collier and Thome (1994).

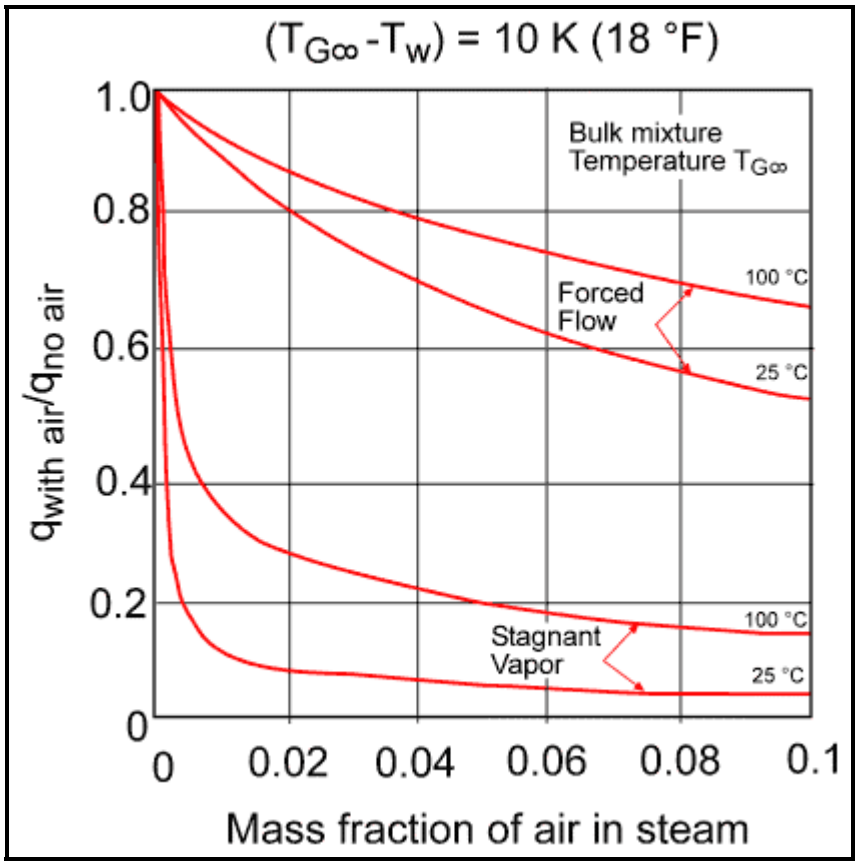

Figure 7.29. Condensation of steam in the presence of air [taken from Collier and Thome (1994)].

Example Calculation: Assume R-134a is condensing on the outside of a 25.4 mm diameter, horizontal low finned tube, where the diameter at the fin tips is 25.4 mm, at its saturation temperature of 40°C. The tube wall temperature is 35°C. The tube has the following external dimensions: 1000 fins/meter, fin height of 1.5 mm, fin thickness of 0.3 mm and fin tip diameter of 25.4 mm. The fins can be considered to be rectangular in profile and without fouling. The thermal conductivity of the tube is 390 W/m K. Using the Beatty-Katz method, determine the heat transfer coefficient for the tube based on the effective area, the nominal heat transfer coefficient and the condensate retention angle.

Solution: The necessary physical properties at 40°C are:

ρ_L = 1147 kg/m^3; ρ_G = 50.0 kg/m^3; μ_L = 0.000183 Ns/m^2; h_{LG} = 162900 J/kg; λ_L = 0.0776 W/mK; c_{pL} = 1.508 kJ/kgK; σ = 0.0061 N/m.

Using [7.2.19] to include subcooling of the condensate in the heat balance:

$$h'_{LG} = 162900\left[1 + 0.68\left(\frac{1508(40-35)}{162900}\right)\right] = 162900\left[1 + 0.0315\right] = 168027\ \mathrm{J/kg}$$

D = 25.4 mm or 0.0254m and the root diameter D_{root} = 22.4 mm = 25.4 – 2(1.5) or 0.0224 m. Per meter of tube, A_{root} is the surface between the fins, such that for 1000 fins per meter (fpm):

$$A_{root} = fpm\left(s - t_{root}\right)\left(\pi D_{root}\right) = 1000\left(0.001 - 0.0003\right)\pi(0.0224) = 0.04926\,m^2$$

A_{fin} is the fin surface area per meter of tube including the tip area:

$$A_{fin} = A_{sides} + A_{tip} = 2\,fpm\,\pi\left(\frac{D^2 - D_{root}^2}{4}\right) + fpm\,\pi\,D\,t_{tip}$$

$$= 2(1000)\pi\left(\frac{(0.0254)^2 - (0.0224)^2}{4}\right) + 1000\,\pi\,(0.0254)(0.0003)$$

$$= 0.22525 + 0.02394 = 0.24919\,m^2$$

A_{total} is the total area per unit length of finned tube:

$$A_{total} = A_{root} + A_{fin} = 0.04926 + 0.24919 = 0.29845\,m^2$$

The equivalent length of the fin is obtained with [7.7.11]:

$$L_{fin} = \frac{\pi\left((0.0254)^2 - (0.0224)^2\right)}{4(0.0254)} = 0.004434\,m$$

The heat transfer coefficient on the sides of the fin is obtained with [7.7.12]:

$$\alpha_{fin} = 0.943\left[\frac{1147(1147 - 50)(9.81)(0.0776)^3(168027)}{0.000183(0.004434)(40 - 35)}\right]^{1/4} = 3707.3\ W/m^2K$$

On the root area, the heat transfer coefficient is obtained with [7.7.10]:

$$\alpha_{root} = 0.725\left[\frac{1147(1147 - 50)(9.81)(0.0776)^3(168027)}{0.000183(0.0224)(40 - 35)}\right]^{1/4} = 1901.2\ W/m^2K$$

The parameter m in the fin efficiency is obtained with [7.7.9]:

$$m = \left[\frac{2\left(\frac{1}{3707.3} + 0\right)^{-1}}{390(0.0003)}\right]^{1/2} = 251.74$$

The fin efficiency η_{fin} is obtained with [7.7.8]:

$$\eta_{fin} = \frac{\tanh\left[251.74\left(0.0015+\frac{0.0003}{2}\right)\right]}{251.74\left(0.0015+\frac{0.0003}{2}\right)} = 0.946$$

The surface efficiency $\eta_{surface}$ is then obtained with [7.7.7]:

$$\eta_{surface} = 1-\frac{0.24919}{0.29845}(1-0.946) = 0.955$$

The effective heat transfer coefficient for the finned tube is obtained from [7.7.5]:

$$\alpha(0.955) = 1901.2\left(\frac{0.04926}{0.29845}\right)+3707.3\left(\frac{0.946(0.24919)}{0.29845}\right) = 313.8+2928.2 = 3242.0$$

$$\alpha = 3242/0.955 = 3395 \text{ W/m}^2\text{K}$$

The effective surface area is:

$$A_{eff} = \eta_{surface}A_{total} = A_{root}+\eta_{fin}A_{fin} = 0.04926+0.946(0.24919) = 0.285\text{m}^2$$

The nominal heat transfer coefficient is:

$$\alpha_{nom} = \alpha\left(\frac{A_{eff}}{\pi DL}\right) = 3395\left(\frac{0.285}{\pi(0.0254)(1.0)}\right) = 12126 \text{ W/m}^2\text{K}$$

The comparable value for a plain tube of the same diameter was 1850 W/m^{2}K. The condensate retention angle is obtained with [7.7.14], where φ is equal to 0 for a rectangular fin, and the intertube fin spacing b = 0.001 - 0.0003= 0.0007 m, so:

$$\beta = \cos^{-1}\left\{1-\left(\frac{4(0.0061)\cos(0)}{1147(9.81)(0.0007)(0.0254)}\right)\right\} = 0.499 \text{ radians or } 28.6°$$

Thus about 16% of the circumference of the finned tube retains condensate between the fins.